

# Design of a target lock for an endoscope using TeleFLEX

S.D. (Stefan) Frijnts

MSc Report

**Committee:**

Prof.dr.ir. S. Stramigioli  
Dr.ir. F. van der Heijden  
N. van der Stap, MSc  
Dr. R. Reilink

November 2015

031RAM2015  
Robotics and Mechatronics  
EE-Math-CS  
University of Twente  
P.O. Box 217  
7500 AE Enschede  
The Netherlands



## Abstract

Flexible endoscopy is used to examine internal body cavities. A flexible endoscope consists of a flexible tube with a camera in the tip. The tip of the endoscope can be bend to steer the flexible endoscope i.a. during insertion. It is important that the endoscope stays focused on the working area during a clinical procedure. This requires continuously steering of the endoscope because the environment is not fixed. The aim of this project is to add a target lock to the TeleFLEX set-up. The target lock keeps the endoscope camera automatically focussed on a selected target. This is done using the TeleFLEX set-up and the vision algorithm, this vision algorithm is optimised to track a target in internal body cavities. The TeleFLEX is used to robotically steer the endoscope tip.

An endoscope has hysteresis and deadband between steering of the control handle, and movement of the tip. Meaning, the tip does not always responds to the input of the control handle. Hysteresis and deadband limits the performance of target lock. During the project, hysteresis and deadband is measured using OptiTrack and the TeleFLEX set-up. These measurements are combined with research of the working principles of an endoscope, to make a model of an endoscope and the TeleFLEX set-up. The hysteresis and deadband of the model are comparable to a real endoscope.

Different control algorithms are designed, tested in simulations, and integrated on the TeleFLEX set-up. The control algorithms use the vision algorithm to track the selected target and automatically steer the endoscope tip to keep it focussed. One of the control algorithms actively compensate for hysteresis in an endoscope.

The different tracking algorithms are tested, using a special test set-up. The experiments showed the different designed tracking algorithms succeeded to track a target. The test set-up allowed the performance of different tracking algorithm to be compared. Results showed hysteresis compensation can help, further research is required to make it more robust. The experiments on the real TeleFLEX set-up are compared to the designed model of the TeleFLEX set-up, and show the model can be used to predict performance improvements.



# Contents

<b>1</b>	<b>Introduction</b>	<b>1</b>
1.1	TeleFLEX . . . . .	1
1.2	Aim of the project . . . . .	2
1.3	Report structure . . . . .	2
<b>2</b>	<b>Background information</b>	<b>3</b>
2.1	TeleFLEX design . . . . .	3
2.2	Endoscope hysteresis and deadband . . . . .	6
2.3	Control with hysteresis . . . . .	8
2.4	Vision algorithm . . . . .	9
<b>3</b>	<b>Modelling the target lock</b>	<b>10</b>
3.1	New hysteresis and deadband measurement system . . . . .	10
3.2	Endoscope model . . . . .	12
3.3	TeleFLEX model . . . . .	22
3.4	Model parametrization . . . . .	23
3.5	Model results . . . . .	25
3.6	Summery . . . . .	27
<b>4</b>	<b>Control design and implementation</b>	<b>29</b>
4.1	Vision algorithm integration . . . . .	29
4.2	PI control algorithm with hysteresis suppression design . . . . .	30
4.3	Inverse kinematics design . . . . .	32
<b>5</b>	<b>Experimental design</b>	<b>35</b>
5.1	Target design . . . . .	35
5.2	PI parameter estimation . . . . .	36
5.3	Controller performance verification . . . . .	36
<b>6</b>	<b>Expirment results</b>	<b>38</b>
6.1	PI parameters . . . . .	38
6.2	Target lock and model validation . . . . .	38
6.3	Different tracking algorithm performances . . . . .	40
<b>7</b>	<b>Conclusion</b>	<b>44</b>
<b>8</b>	<b>Discussion and recommendations</b>	<b>45</b>
	<b>Bibliography</b>	<b>47</b>



# 1 Introduction

Flexible endoscopy is used to examine internal body cavities. A flexible endoscope consists of a flexible tube with a camera on the tip. The tip of the endoscope can be bend to steer the flexible endoscope i.a. during insertion. Most endoscopes have one working channel, this channel is used to insert different instruments into the body cavity. For example this can be used for biopsy.

Physicians are experimenting to use endoscopy for more advanced procedures, this is costly in physicians working hours. There is a lot of time loss in positioning the endoscope before it can be used. Conducting a procedure using only one instrument is quite difficult, and not very efficient. When two instruments can be used in one endoscope, it will benefit the efficiency of the procedure. For example, one instrument can be used for holding, while the second instrument can be used for cutting. Using multiple instruments requires the physician to control the endoscope and instruments at the same time. This requires multiple physicians to control the different instruments. Robotic steering should help by making the endoscope and instruments better controllable.

## 1.1 TeleFLEX

Endoscopes have control handles to steer the tip of the endoscope. The endoscope used in the TeleFLEX project has a tip which can be steered in two directions. The control handle of the endoscope is not very intuitive. This makes it difficult to control the tip of the endoscope by one hand.

The University of Twente in collaboration with Demcon has designed a robotic steering device for endoscopes. The steering device and the project are both called TeleFLEX. The design is based on reusing existing endoscopes, by mounting it on robotically controlled steering modules. TeleFLEX makes the tip control more intuitive and ergonomic using a digital input module, to robotically control the endoscopes control handles [14].



**Figure 1.1:** The TeleFLEX setup. An endoscope is mounted in the steering module which can be seen in the right..

The camera in the tip of the endoscope can be connected to the TeleFLEX system to automate steering of the tip. This is currently used for automatic steering during insertion of the endoscope [15].

## 1.2 Aim of the project

It is important that the endoscope stays focused on the working area during a clinical procedure. This requires continuously steering of the endoscope because the environment is not fixed. The aim of this project is to add a target lock to the TeleFLEX set-up. The target lock should keep the endoscope tip focused on the selected target during the procedure. The endoscope camera will be used to track the relative motion between the endoscope and the environment. This tracking information is used to automatically steer the endoscope tip to keep it focused on the target. The target lock should be easy to use and will be integrated in the current TeleFLEX set-up.

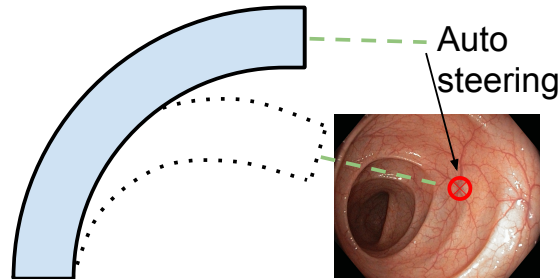


**Figure 1.2:** Auto steering bends the endoscope and keeps the target (in red) automatically in focus. Target is tracked using the vision algorithm.

## 1.3 Report structure

The first step was getting insight into the current TeleFLEX set-up. This was needed as the target lock needed to be integrated. The beginning of chapter two gives an technical overview of the TeleFLEX set-up.

Endoscopes have hysteresis and deadband, this results in the tip of the endoscope might not directly respond to the control handle. This limits the performance of the target lock. A measurement set-up and produce was available to measure the hysteresis and deadband. Information on hysteresis, deadband and the measurement produce will be given in the end of chapter two.

The third chapter a new measurement procedure is introduced, which combines the OptiTrack and TeleFLEX to measure hysteresis and deadband using an Olympus endoscope. These measurements are used to make a model of the endoscope and TeleFLEX set-up using bond graph. The final model is parametrized to have the same deadband and hysteresis of the endoscope. This model is used to test different control algorithms.

In the fourth chapter, three different auto-steering algorithm designs are given. The control algorithms use the vision algorithm as steering input, to keep the target central in the image plane. The control algorithms are designed and tested in simulations, and integrated in the real TeleFLEX set-up.

An experimental set-up to validate and measure the performance of the auto-steering algorithms, is described in chapter five. The experimental results can be found in chapter six. Conclusions, discussion, and recommendations are presented in chapter seven and eight.

---

## 2 Background information

The background information is divided in two sections. The first part gives information on the TeleFLEX design. This information is used for modelling and integrating the auto steer algorithm in the TeleFLEX set-up. The second part contains details on hysteresis and deadband of the endoscope.

### 2.1 TeleFLEX design

The TeleFLEX is designed to be portable and easy to use. The TeleFLEX set-up consists of three control modules for robotic steering of the complete endoscope. The first two modules are used for steering the endoscope itself. The third module is used for manipulation of the instruments inserted through the endoscope.

#### 2.1.1 Endoscope steering

The Endoscope steering is build out of two modules. The first module controls the tip of the endoscope and can be plugged onto the endoscope control handle. This module is designed to be small and flexible to stay out of the way during surgery. The second module controls the endoscope itself. This module can be mounted after insertion of the endoscope and can control the endoscope in axial and rotation direction. This module can be used during control of the instruments which helps the physician by making the complete endoscope controllable with one hand.

#### 2.1.2 Instrument steering

The TeleFLEX support multiple instruments which can be inserted through the endoscope or mounted externally. The instruments have special designed standardized control interfaces which can be mounted on the TeleFLEX. This set-up allows the TeleFLEX to control different instruments.

Instruments have a small working area where they have to be accurately controlled. Instruments use the same actuation principles as an endoscope with the same hysteresis problems. This makes it difficult to precisely control the instruments. Robotic steering can be used to overcome these hysteresis problems. This requires knowledge about the hysteresis. Previous research has focused on optical feedback and reverse kinematics to measure the hysteresis while controlling the instruments. This can reduce the hysteresis with 70%, using active feed forward control. This method has never been implemented on the real TeleFLEX set-up [12].

#### 2.1.3 TeleFLEX control design

The TeleFLEX set-up has multiple motors and encoders to steer the endoscope and instrument steering modules. These motors are all controlled using motor controllers, called Elmo's. Elmo's are configured to run in position mode, using the motor encoder and a PID controller. The Elmo runs the PID control loop, real time, at a high speed. Elmo's are motion controllers generating a motion path for steering to the position setpoints. This path can be configured with several parameters, for example maximum velocity or acceleration. This can create a gap between the setpoint of the TeleFLEX set-up and actual angle of the motor when the maximum velocity of the path generator is too low. This should be taken into account, designing a control setpoint generating algorithm.

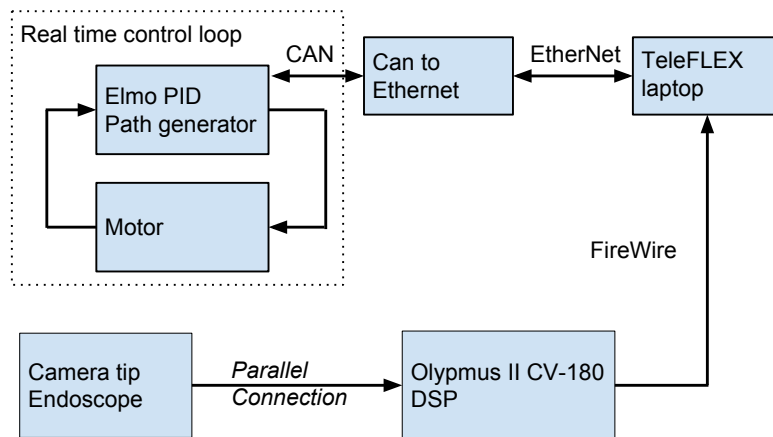


**Figure 2.1:** Systematic overview of the teleFLEX set-up. On the left are the motion controllers which drives the different steering modules on the TeleFLEX set-up. A specially made adapter allows the communication between the TeleFLEX laptop and Elmo using Ethernet to Control Area Network. The camera of the endoscope tip is connected to a video encoder which codes the video signal to FireWire. Firewire can be plugged into a laptop.

The Elmo's motor controllers communicates over the Controller Area Network (CAN). A special adapter translates the CAN network to standard TCP/IP Ethernet which can be connected to a normal laptop or computer. The TeleFLEX software runs a control loop which can sent position commands to the TeleFLEX motor controllers.

The camera of the endoscope is connected to the video processing unit, the Olympus II CV-180. The Olympus II CV-180 does the first image filtering, i.a. white balancing, and translates the endoscope camera interface to FireWire. The FireWire is connected to the laptop to be used for control.

#### 2.1.4 TeleFLEX software design

The TeleFLEX software is programmed in Python. The TeleFLEX has special designed input devices that to control the endoscope. The software uses these input devices to generate setpoints. The TeleFLEX software generated setpoints are send to the Elmo motor controllers. These setpoints are the input for the Elmo control loop, steering the control handle of the endoscope. The TeleFLEX software itself contained more then 3000 lines, and documentation was limited to in-line comments. One of the first steps in the project was getting an overview of this code so it could be used to add functionality.

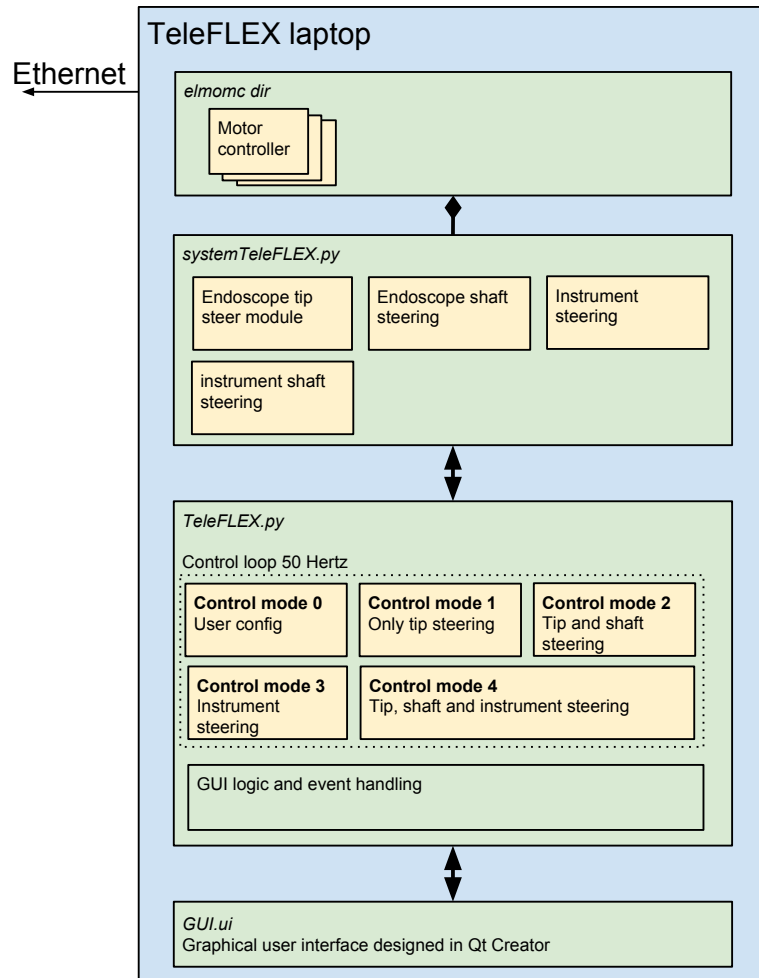


**Figure 2.2:** Control software running on the laptop.

The endoscope steering unit, endoscope shaft manipulator, and instruments are abstracted into separated modules. These modules contain their own logic for homing, setting and getting positions. These modules also contain the safety layers to prevent the endoscope from steering before homing and limits the setpoint range. To control the TeleFLEX, these modules use Elmo motor controllers, which are abstracted into a class. This class can be used to send commands and receive information from the Elmo command interface over the Ethernet. The Elmo's are assigned to different modules. This allows the modules to control their own motors.

The TeleFLEX has a timer which drives the control loop at 50 hertz. This timer is split up in different control modes. Most of these control modes are coupled to the different tabs in the Graphical user interface (GUI). Each control mode uses steering modules to send setpoints to the TeleFLEX. The best way found for adding functionality to the current TeleFLEX, is to add a tab to the GUI. The tab is coupled to a separated control mode in the timer loop. Within this mode in the timer loop, the different control modules method can be used control the endoscope or instruments. This means all the safety functions are still used. This method gives a high integration in the current TeleFLEX set-up. The added GUI tab is extended to test different parameters without complete restarting the software.

## 2.2 Endoscope hysteresis and deadband

The tip of an endoscope can be steered for insertion, examination and small interventions. A control handle on the endoscope can be used to steer the tip. Rotating the control handle does not always result in steering of the endoscope tip.

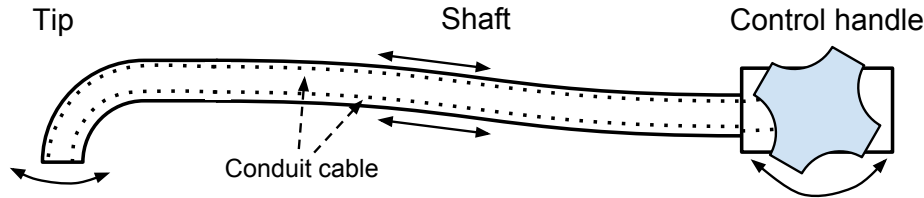


**Figure 2.3:** Endoscope overview. The arrows gives the movement of the control handle, conduit cables and tip.

The endoscope tip is steered with two conduit cable pairs, as shown in Figure 2.3. The tip itself is designed to have low bending stiffness and high compression stiffness. Two conduit cables which are connected to the tip can pull the tip at an angle. The conduit cables are guided through the shaft of the endoscope to the control handle. Each conduit cable pair controls one degree of freedom of the tip. The mechanical design is optimised to be as small as possible. The mechanical driving principle causes hysteresis and deadband between the control handle and tip.

For measuring the hysteresis and deadband, a special TeleFlex set-up and measurement procedure exist. The set-up consists of an external camera which is positioned above the endoscope looking downward. The external camera is used to track the tip position in two dimensions, and is connected to the TeleFLEX set-up. The endoscope tip is controlled using the TeleFLEX set-up. It is connected to the TeleFLEX laptop. This allows the TeleFLEX laptop to steer the control handle of the endoscope while keeping track of the endoscope tip position.

The hysteresis and deadband measurement procedure consists of slowly moving the control handle of the endoscope from left to right. The rotation angle of the control handle is set larger after each cycle. The tip follows this movement, with some delay depending on the hysteresis and deadband. To show the effect of hysteresis and deadband the tip position is plotted against the control handle angle.

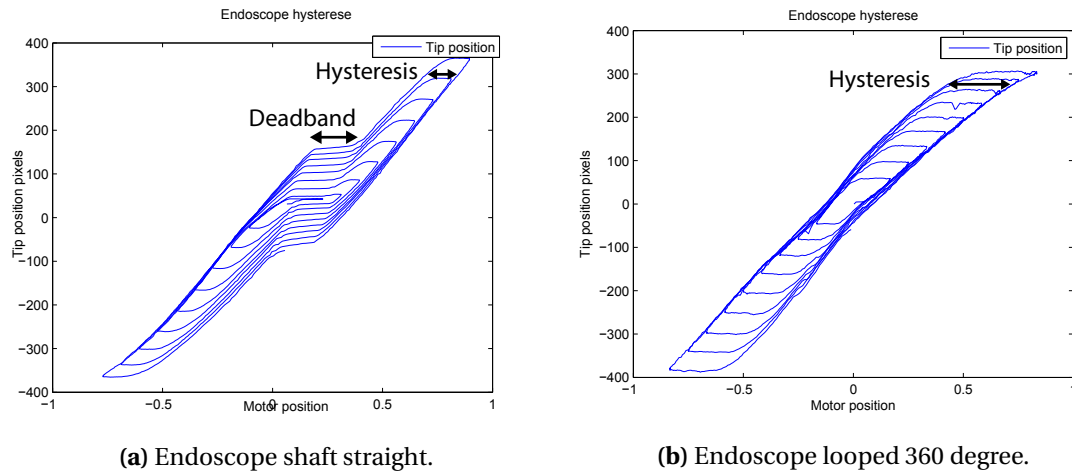


**Figure 2.4:** Hysteresis measurements taken from an endoscope. The hysteresis can be seen as the difference between the path that returns the tip to the center, compared to the path which pulls the tip under at an angle. The deadband is visible in the center of the left plot.

Two measurements taken with this set-up, are shown in Figure 2.4. The left measurement is taken when the endoscope shaft is laid straight, in the right measurement the endoscope shaft is laid down in a 360 degree loop. There are some clear differences between these measurements.

The left measurement in Figure 2.4 shows an extra straight part in the center. This is identified as deadband. It is created by slack in the conduit cable pairs which drive the endoscope tip. The tip itself can be seen as a spring to keep tension on one cable until it reaches the center. In the center, the other cable needs to start pulling to go in the other direction. This results in the control handle being rotated while the tip is not moving until the cable slack is gone. Deadband is visualised in Figure 2.5. The deadband disappears if the endoscope is laid in a 360 degree loop as can be seen in Figure 2.4a.

The upper right and bottom left phenomenon in both plots Figure 2.4 is called hysteresis. This is measured when the control handle changes direction. The tip centring force keeps one conduit cable tensioned while bending in one angle. This results in one conduit cable actuating one bending angle in both directions as shown in Figure 2.5. The measurements show the tip stag-nates for a short moment after the control handle changes direction, the tip starts moving again when the control handle continues to move. Hysteresis measurements also show the hysteresis gets slightly wider if the tip angle increases. More information in hysteresis will be given in Chapter 3.

Not only the disappearance of the deadband can be seen when the endoscope is laid in a 360 degree loop (Figure 2.4a), widening of the hysteresis can be seen as well (Figure 2.4a). The centring force of the tip can be felt even if the endoscope is looped. This means the deadband is not moved to the hysteresis as the tip keeps one conduit cable tensioned. A possible explanation of the disappearance of the deadband will be given in Chapter 3.

Research has been done to hysteresis and deadband of different endoscopes. This shows that the hysteresis and deadband is not consistent between different endoscopes [13].

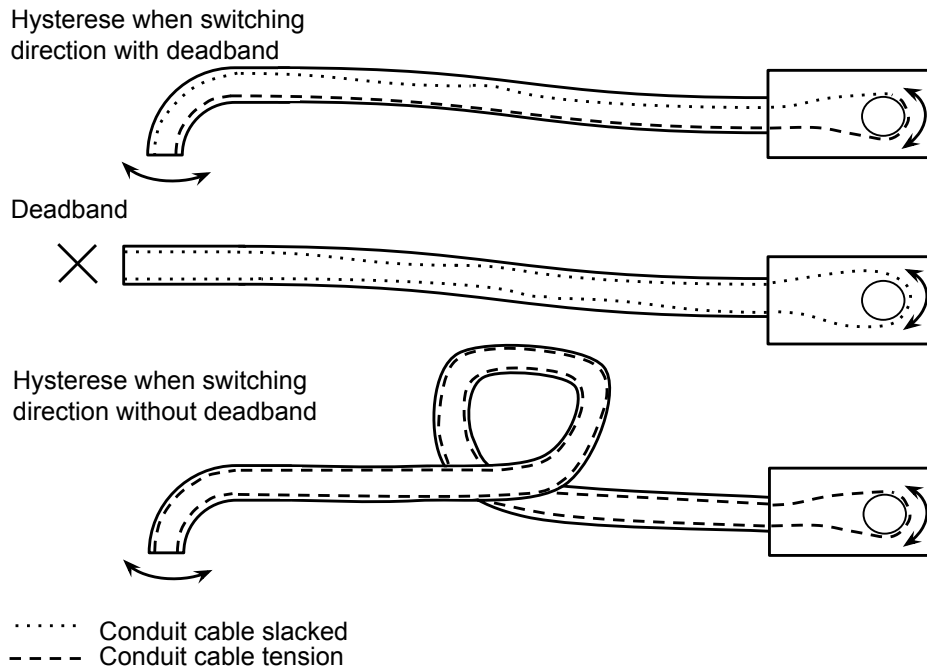


**Figure 2.5:** The top shows the tip position where hysteresis occurs. If the control handle switches direction, the tip stops reacting until the hysteresis effect is gone. The middle shows the tip in the position where deadband is visible as both conduits are slacked. The lowest situation visualised the endoscope being looped. This shows the hysteresis is getting wider and deadband disappears.

### 2.3 Control with hysteresis

Literature shows [12, 10, 4] the most common problem with controlling an endoscopes and instruments, is hysteresis and deadband. Hysteresis is a common problem for bad performing control algorithms. Because of the hysteresis or deadband the output does not immediately respond to the input. Most control algorithms anticipate by increasing the steering values. When the hysteresis or deadband is overcome the input gain is too high and overshoots the target position, and the steering direction has to switch again.

Standardized control solution use specially designed algorithms to identify the hysteresis and compensate for it using feed forward control. This automatic hysteresis identification process is slow, due to the fact that hysteresis is depending on the previous state of the system. This creates practical problems as hysteresis of the endoscope changes any time and is also depending on the endoscope shaft position. This means, hysteresis measurement needs to be done every time the endoscope is used. This is not practical and can not be used in a clinical setting.

## 2.4 Vision algorithm

An special designed vision algorithm used to track a target with the camera [17]. The output of the vision algorithm is the x and y position of the target in the image plane. This algorithm needs to be fast enough to be usable to control the tip. The tracking algorithm uses OpenCL implementation on a GPU to accelerate tracking algorithms. The output of the vision algorithm is used as input for steering the tip to automatically to keep the working area in focus. An overview of the vision algorithm can be found in Figure 2.6.

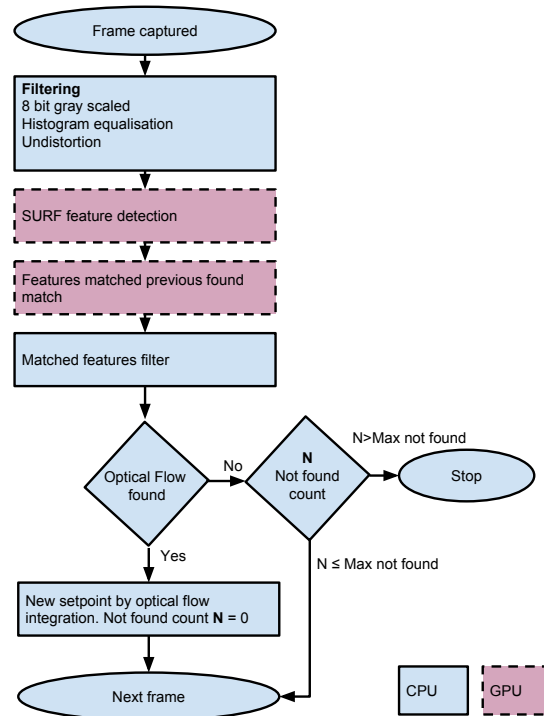


**Figure 2.6:** A short overview of the vision algorithm used on the TeleFLEX set-up. The input is filtered. The SURF algorithm is used to find features of the captured image. Features are matched to the previous frame where the target was found. The found match of the features are filtered. Depending on the outcome of the filtering, the optical flow is accepted or rejected. The Maximum not found can be configured. The different colors and lines indicates if the step is done using the CPU, or is accelerated using the GPU.

### 3 Modelling the target lock

Hysteresis and deadband make an accurate and responsive control of the endoscope tip difficult. Hysteresis and deadband can be measured using the special designed measuring procedure. However the physical cause of hysteresis is not entirely clear. A model of the endoscope is designed to get better insight in the deadband and hysteresis and how it influences the control performance. Research has shown that hysteresis and deadband changes between endoscopes, and within one endoscope between different degrees of shaft bending [13]. The model is also used to test different control strategy's. This means, the complete control loop, including the camera and TeleFLEX set-up, is modelled, using 20-sim.

Making a model of the endoscope was difficult as it is not possible to tear the endoscope down without damaging it. Therefore modelling of the endoscope has been done in multiple phases. In the first phase a new measurement system is introduced to get more information on the deadband and hysteresis of the endoscope. The second phase is splitting the endoscope in three parts: the control handle, the shaft and the tip of the endoscope. For each part the effects which play a role in hysteresis and deadband is analysed. The separated parts are coupled together and simulated in 20-sim. The endoscope model is parametrized using the hysteresis and deadband measurements. In the last phase the TeleFLEX, which steers the endoscope, is modelled and connected to the endoscope. This allows the control algorithm for the target lock to be tested in a simulation.

#### 3.1 New hysteresis and deadband measurement system

The old measurement set-up for hysteresis and deadband measuring used an external camera which filmed the endoscope. The tip was tracked using this external camera while the tip was moved from the left to the right with increasing angles. Plotting the tip position against the input control handle showed hysteresis curves as shown in Figure 2.4. The limitation of this set-up was that only one tip direction could be analysed. Secondly the set-up was rather slow as each picture needed to be analysed before continuing with the next measuring position of the control handle.

The new measurement system uses the OptiTrack measurement system. The OptiTrack system uses multiple cameras with infra-red light, reflective balls, and special software. The cameras are used to track reflective balls to calculate the 3D coordinates using special software. Multiple balls can be combined in a single frame in the OptiTrack software, to track the position and orientation of this frame.



**Figure 3.1:** The holder for the OptiTrack balls which is mounted on the tip of the endoscope. The design is optimised for 3d printing, it consists of two parts which are identical and can be printed without overhang. The inner diameter is wider around the pivot and clam, preventing any damage to the endoscope during tightening. The shaft with the OptiTrack balls are modular to test different configuration such as lengths. The final shafts are made from aluminium limiting the weight.

A special holder for the endoscope tip is prototyped using 3D printing. This holder allows multiple OptiTrack balls to be attached to the tip of the endoscope as show in Section 3.1. The OptiTrack software sends out a bitstream over a socket connection using TCP with pose information of the grouped optiTrack balls. A Python package for receiving and encoding the OptiTrack bitstream is available and is adapted work with an older version of OptiTrack, used on the University [2].

Hysteresis and deadband are measured using the motor position of the TeleFLEX set-up and the tip position is measured using the OptiTrack measurement system. This means both measurement systems needs to be synchronised to get correct measurements. This is accomplished by integrating the OptiTrack bitstream encoder, using the parallel processing package of Python. The parallelization allows the bitstream from the OptiTrack to be encoded without being interrupted by the TeleFLEX software. The standard connection between two Python processes, the OptiTrack encoder and TeleFLEX software, is buffered. This is problematic as the OptiTrack measures faster compared to the TeleFLEX control loop. This fills the buffer faster than it can be read out. This problem is solved by clearing the buffer before putting a new value in. This creates a blocking non-buffer communication between the two processes.

The main focus of the new hysteresis and deadband measurement using the OptiTrack, is to check if the bending of the tip is influenced by the hysteresis from the other bending direction. The old hysteresis and deadband measurement procedure where the tip was moved from left to right with increasing angles, gave good results and is reused. For the new measurements the second bending angle is increased for each measurement. The hysteresis final plot is obtained by calculating the angle between the tip and the base,  $\Phi$ , as shown in Figure 3.7a and plotting it against the motor position. This required a second set OptiTrack balls, positioned at the base of the endoscope tip. The final plot is shown in Figure 3.2.

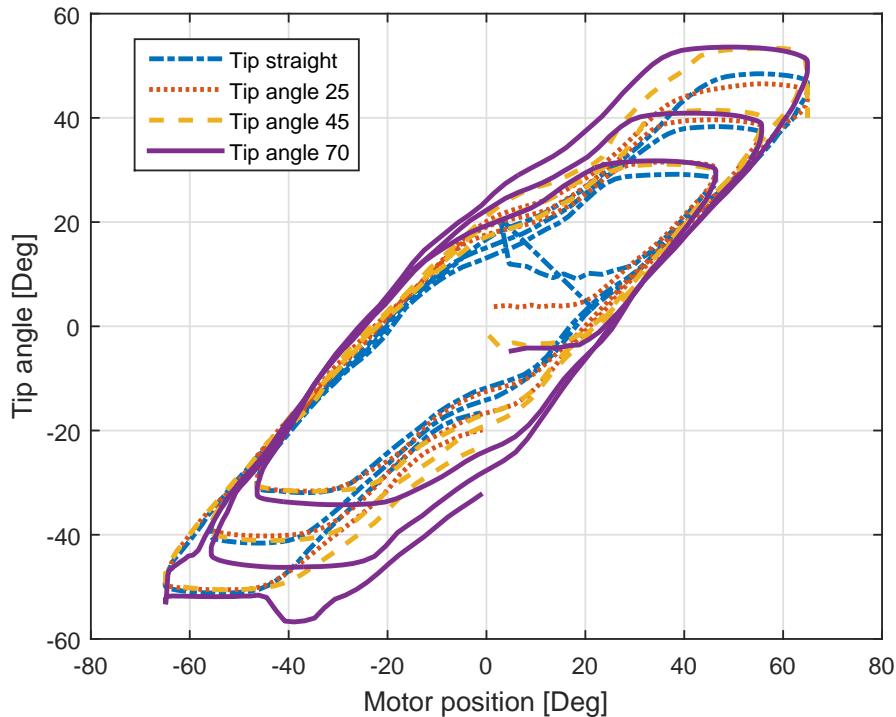


**Figure 3.2:** The figure contains four measurements each with a different angle of the tip which is not moving. This hysteresis measurement shows that the tip hysteresis is depending on the set angle in the other direction. The starting point of each measurement is in the center and the line rotates counter clock wise.

The measurement is done with a recently calibrated endoscope. This is clearly visible as the deadband is almost gone in the center while the endoscope is lying on a flat table top. For each measurement the hysteresis width gets bigger if the angle is increased. This was already visible with the previous measuring set-up in Figure 2.4. This new measurement procedure shows that the hysteresis width is not only depending on the moving tip angle but also on the tip orientation in the other direction. The hysteresis gets wider if the tip angle in the other direction is set at a larger value. It can also be observed that the tip enters the deadband earlier depending on the angle of the not moving direction.

### 3.2 Endoscope model

The first step in modelling the endoscope is splitting it up in three parts. The first part is the control handle which controls the tip. The second part is the conduit cables, which run through the shaft to the tip. The endoscope tip is the third part. Each part will first be discussed separately and then integrated into one model in the last part of this chapter. The input of the endoscope model is the control handle orientation, the output is the tip orientation and position.

For the modelling the endoscope and TeleFLEX 20-sim is used. 20-sim allows the modelling of bondgraphs. Bondgraphs use energy pairs for the relation between different sub parts. The main advantage of 20-sim is that custom elements can be programmed and simulated.

#### 3.2.1 Control handle of the endoscope

The control handle of the endoscope is directly driving the conduit cables. It is modelled as a transformation factor which transforms the rotation to a translation of the conduit cables.

This gives Equation (3.2) where  $\phi_{control}$  is the angle velocity of the control handle,  $T_{control}$  is the control handle torque,  $F_{fc}$  is the tension in the conduit cable and  $V_{begin}$  is the conduit cable velocity in the beginning. The internal radius,  $r$ , translates the control handle rotation to translation of the conduit cable, as shown in Figure 2.5.

$$\tau_{control} = rF_c \quad (3.1)$$

$$\phi_{control} = r v_{begin} \quad (3.2)$$

### 3.2.2 Shaft of the endoscope

The conduit cables, to steer the tip, go through the flexible shaft. This type of steering is popular when the space for the actuator is limited, for example in robotic hands. The use of conduit cables comes at a price. They are not ideal for precise controlling.

The two main problems with conduit cables are friction and stiffness which create hysteresis between input and output position. The third problem with cables is that they can only pull, this is solved by using two conduit cables in a pull pull configuration to control one degree of freedom. This results in deadband when no pretension is applied. Adding too much pretension results in more friction which adds hysteresis.

During the project, the endoscope is recalibrated. This minimized the cable slack without pre-tensioning the conduit cable. The cable slack increases, by using the endoscope under tension, and disinfecting after it was used. The model should take into account that the deadband can be different for each endoscope.

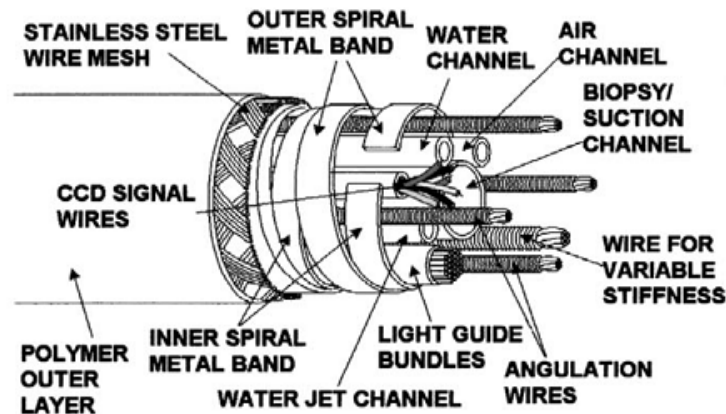
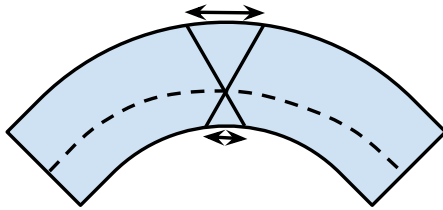


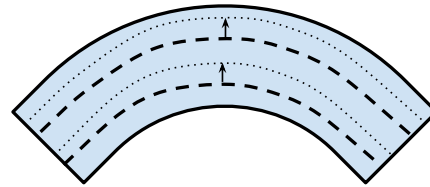
**Figure 3.3:** The insight of an endoscope shaft. It shows that the conduit cables are placed outside the shaft. [16]

Measurement taken with the TeleFLEX set-up showed that the deadband is also depending on the endoscope path. This means that the deadband and pretension changes during an intervention. The deadband becomes less and eventually goes to zero when the endoscope is bended, this is clearly visible in measurement Figure 2.4. The conduit cables are positioned at the outer wall of the endoscope shaft Figure 3.3. Bending the endoscope makes the inner cable path shorter and the outer cables path becomes longer. The measurement showed that the deadband disappeared when the endoscope is bended. This is probably an effect of the inner conduit path becoming less shorter than the outer cable path is becoming longer. A longer path result in the conduit to be stretch while the cables stays the same length due the difference in stiffness between the conduit and cable.

There are possible explanations how the total conduit path becomes longer. The first explanation is the natural bending plane of the endoscope which is not precisely in the middle of the endoscope shaft, due its construction. This results in the described effect of inner and outer cable path length differences. Figure 3.4a. A second explanation could be that the conduit cable pair moves in a way that elongates the total path. For example both conduit cables move to the outside as shown in Figure 3.4b.



(a) Natural bending plane is not in the middle of the endoscope. This result in the inner cable becoming less shorter compared to the outer cable path becoming longer.



(b) Both conduit cable pair move to the outside resulting to the total path becoming longer.

**Figure 3.4:** Possible explanations why the deadband changes due the bending of the endoscope.

The precise effect of bending an endoscope, without looking inside the endoscope shaft, is unknown. A possible explanation for the disappearance of the deadband could be an effect of the changes in path length from the conduit cables. For the model it is assumed that bending the endoscope lowers the cable slack and eventually pretension start to build up when there is no cable slack left. Currently it is not clear what the maximum allowed pretension is, extra pretension of the conduit cables could result in the endoscope shaft becoming shorter or an other unexpected effects.

Hysteresis in conduit cables comes from friction and stiffness. The friction is created by cables sliding against the conduit when going around the corners as shown in Figure 3.5.

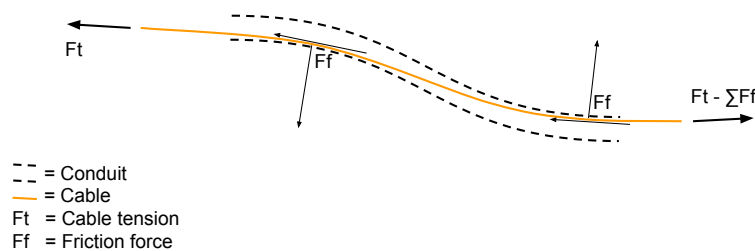


**Figure 3.5:** The friction in a cable conduit is depending on the cable tension. The internal cable is moving to the left, the tension in the cable changes due the friction. The resulting change of force divided by the conduit cable stiffness results in hysteresis in position between the left and right side of the conduit cable.

Modelling this effect ,numeric approaches are used[8, 1, 11]. A numeric approach splits the cable in multiple element which are coupled using springs. Each element has friction between the element and its conduit. A typical static friction model is used, for example the coulomb friction model. The coulomb model assumes that the friction is only depending of the normal force and direction of the element.

Using an numeric modelling approach has some drawbacks. The complete path of the endoscope with the conduit cable has to be known and the resulting models based on this approach are very time consuming to simulate. Laying the endoscope straight as done in the current hysteresis measurement should result in a minimum friction in the conduit cable. These hysteresis measurements however still show a significant hysteresis width. Therefore the model of the conduit cable will be a extremely simplified version of conduit cable. The cable is modelled using a spring with stiffness  $K_{cable}$ .  $v_{begin}$  and  $v_{end}$  are used for velocity at the beginning and end of the conduit cable,  $\Delta L$  for conduit cable change in length and  $L_{t_0}$  for the initial cable length. The spring is modelled in the way that it can only pull by switching the relation between the tension  $F_c$  and cable length  $\Delta L$ . The simplification does not allow the tension  $F_c$  at the beginning of the conduit cable to differ from the end of the cable. The friction depending on the normal force, is modelled with the tip Equation (3.29). This also simplifies the parametrization of the final model.

$$v_{\Delta}(t) = v_{begin} - v_{end} \quad (3.3)$$

$$\Delta L(t) = \int_0^t v_{\Delta}(t) dt + L_{t_0} \quad (3.4)$$

$$F_c(t) = \begin{cases} 0 & \text{if } \Delta L(t) < 0 \\ \Delta L(t)K_{cable} & \text{if } \Delta L(t) \geq 0 \end{cases} \quad (3.5)$$

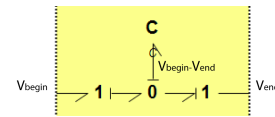


**Figure 3.6:** The 20-sim implements the equations on the left.

Other dynamical effects can play a role with high pretension in conduit cables pairs, controlling one degree of freedom. The conduit cable pairs influence each other. This can give unexpected behaviour[1]. Bardou et al. refers to this as the source of hysteresis in the endoscope [4]. This is incorrect. If there indeed is deadband in the system, there is no pretension between the conduit cables meaning that the model [1] should not be applied. If the endoscope is laid in a loop the deadband disappears as shown in Figure 2.4. This create pretensions between the conduit cables, meaning the model of Agrawal et al. [1] can be used. Their result shows the effect should be visible while moving the tip in one direction. The currents hysteresis and deadband measurements does not show this effect, and is neglected in the model of the shaft.

### 3.2.3 Tip of the endoscope

The tip model is split in two parts. The first part is the feed forward kinematic which gives the tip its position and orientation with respect to the base depending on the conduit cable position at the end. In the second part the internal friction is added to the model.

The tip position of an endoscope and instruments is mostly modelled by assuming a constant curve [3, 12, 10]. For modelling, the Denavit Hartenberg notation is preferred, used by Bardou et al.[3], based on Hannan et al.[7]. They used the Denavit Hartenberg forward kinematics for calculating the forward kinematics of the tip in one plane. They switch to 3D by rotating the base around the axis. This approach can give the correct position of the endoscope tip, but does not give the correct orientation. To solve this the tip is split into multiple joints which bend around one axis with a constant curve. The joints alternate between the bending axis creating the two bending degrees of freedom. The chain of the elements gives the forward kinematics of the end of the tip with respect of the base. This mechanise is also described by Kitagawa et al. in the patent of a flexible steered endoscope tip [9].

The first step is to calculate the forward kinematics of a joint with constant curve in a plane. This is done using the screw theory. The unit twist between two frames with a rotational joint can be given by Equation (3.6), where  $\hat{\omega}$  is the rotation vector and  $\hat{v}_1$  is the vector to this rota-

tional axis [12].

$$\hat{T}_1^{2,2} = \begin{bmatrix} \hat{\omega} \\ \hat{v}_1 \wedge \hat{\omega} \end{bmatrix} \quad (3.6)$$

The tip rotation vector  $\hat{\omega}$  is given by a rotation around the y axis as shown in Figure 3.7a, this gives Equation (3.7). By assuming the bend is constant the rotation axis  $\hat{v}$  can be written as Equation (3.8), where  $L$  is the tip length and  $r$  the radius as shown in Figure 3.7a.

$$\hat{\omega} = \begin{bmatrix} 0 \\ 1 \\ 0 \end{bmatrix} \quad (3.7)$$

$$\hat{v}_1 = \begin{bmatrix} 0 \\ 0 \\ r = \frac{L}{\Phi} \end{bmatrix} \quad (3.8)$$

$$(3.9)$$

The transformation between the two frames can be written, using the unit twist.

$$H_2^1 = e^{T_1^{2,2}\Phi} \quad (3.10)$$

This can be calculated using the Rodriguez formula. This can be worked out in Equation (3.12) which gives the rotation matrix around the y axis and Equation (3.13) the translation of the tip in one bending axis.

$$R_2^1 = e^{\omega} = R_y \quad (3.11)$$

$$v_2^1 = (I - R_2^1)v \quad (3.12)$$

$$H_2^1 = \begin{bmatrix} R_2^1 & v_2^1 \\ 0 & 1 \end{bmatrix} \quad (3.13)$$

This results in the following equations for the forward kinematic in a plane around the x and y axis. This is only valid for  $\Phi_x, \Phi_y$  unequal to zero.

$$H_2^1(\Phi_{y_2^1}, L_2^1) = \begin{bmatrix} \cos(\Phi_{y_2^1}) & 0 & \sin(\Phi_{y_2^1}) & (1 - \cos(\Phi_{y_2^1}))\frac{L_2^1}{\Phi_{y_2^1}} \\ 0 & 1 & 0 & 0 \\ -\sin(\Phi_{y_2^1}) & 0 & \cos(\Phi_{y_2^1}) & \sin(\Phi_{y_2^1})\frac{L_2^1}{\Phi_{y_2^1}} \\ 0 & 0 & 0 & 1 \end{bmatrix} \quad (3.14)$$

$$H_2^1(\Phi_{x_2^1}, L_2^1) = \begin{bmatrix} 1 & 0 & 0 & (-1 + \cos(\Phi_{x_2^1}))\frac{L_2^1}{\Phi_{x_2^1}} \\ 0 & \cos(\Phi_{x_2^1}) & -\sin(\Phi_{x_2^1}) & 0 \\ 0 & \sin(\Phi_{x_2^1}) & \cos(\Phi_{x_2^1}) & \sin(\Phi_{x_2^1})\frac{L_2^1}{\Phi_{x_2^1}} \\ 0 & 0 & 0 & 1 \end{bmatrix} \quad (3.15)$$

For  $\Phi_x, \Phi_y$  equal to zero results in:

$$H_2^1(L_2^1) = \begin{bmatrix} 1 & 0 & 0 & L_2^1 \\ 0 & 1 & 0 & 0 \\ 0 & 0 & 1 & 0 \\ 0 & 0 & 0 & 1 \end{bmatrix} \quad (3.16)$$

The forward kinematics for the tip is given by linking Equations (3.14) and (3.15). This results in Equation (3.20) where  $\Phi_y, \Phi_x$  are the total bending around the y and x axis, L the total tip length and the tip is split in n elements. The total bending is divided over the elements.

$$L_2^1 = \frac{L}{2n} \quad (3.17)$$

$$\Phi_{y_2^1} = \frac{\Phi_y}{n} \quad (3.18)$$

$$\Phi_{x_2^1} = \frac{\Phi_x}{n} \quad (3.19)$$

$$H_t^b = \prod_{i=1}^{i=n} H_2^1(\Phi_{x_2^1}, L_2^1) H_2^1(\Phi_{y_2^1}, L_2^1) \quad (3.20)$$

The accuracy of this model compared to single degree of freedom constant curve is depending on the amount of elements the tip is split into. The solution, using a constant curve approach for one degree of freedom in one plane, is known Equation (3.14). This is used to validated the chained forward kinematics. For both Equations (3.14) and (3.20) the position and angel of the tip is calculated between angle -135 to 135 degrees for an endoscope tip of 12cm. For the chained model, 30 elements are used, this gives a maximum position offset of less then 2mm between the two frames and a zero orientation error.

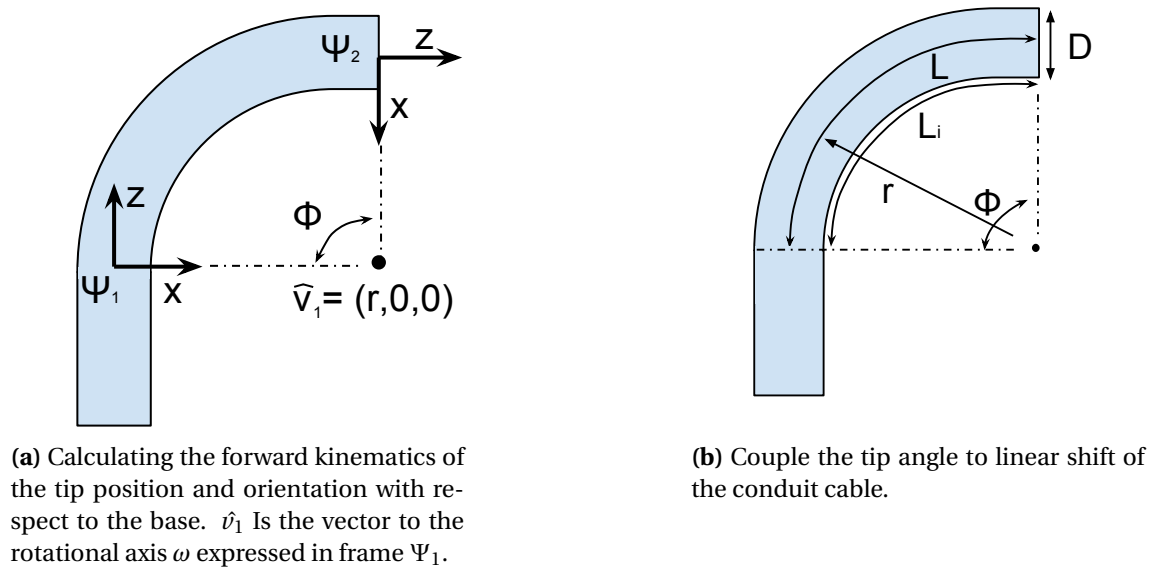


**Figure 3.7:** Forward kinematics of the endoscope tip.

The tip forward kinematics is expressed using a chain of H matrices which bends alternating around their x or y axis Equation (3.20). The model gives the tip position, depending on the two bending angles. These bending angles need to be coupled to the conduit cable position. The relation between the pulling of the conduit cable and tip orientation can be calculated using straight forward geometry Figure 3.7b. The radius  $r$ , endoscope length and angle  $\Phi$  can be written by using the constant curve assumption

$$r = \frac{L}{\Phi} \quad (3.21)$$

It can be seen that the internal radius  $r_i$  depends on the diameter  $D$  of the endoscope and length of the tip. The expression for angle  $\Phi$  depending on  $D, r_i, L$  is given.

$$L_i = (r - \frac{D}{2})\Phi \quad (3.22)$$

$$L_i = L - \frac{D}{2}\Phi \quad (3.23)$$

$$\Phi = (L - L_i) \frac{2}{D} \quad (3.24)$$

Note the above equation actual gives the angle  $\Phi$  depending on the change of conduit cable length  $\Delta L_{tip}$ .

$$\Delta L_{tip} = (L - L_i) \quad (3.25)$$

$$\Phi = \Delta L_{tip} \frac{2}{D} \quad (3.26)$$

Equation (3.26) shows their is a linear relation between the conduit cable position and tip orientation. The calculation is only done for 2D situation. The four conduit cables are distributed radial, under angles of 90 degrees. This means the conduit pairs do not influence each other while being bended. This can be seen in Figure 3.8b, where the conduit cable pair, which bends the tip around the other angle, is in the middle of the tip and does not change its length with the bending around  $\Phi$ .

The linear dependency of the tip orientation and conduit cable position, is used to model the transformation from the conduit cable to the tip orientation.  $\phi_{tip}$  is the angular tip velocity and  $\tau_{ctip}$  the torque of the cable on the tip.

$$\tau_{ctip} = \frac{2}{D} F_c \quad (3.27)$$

$$\phi_{tip} = \frac{2}{D} v_{end} \quad (3.28)$$

A geometric model of the tip cannot be used to model the hysteresis effects of the endoscope tip. Therefore a more mechanical model approach of the tip bending is used. The tip bending is controlled by the pulling of the conduit cables. The conduit stops at the first element of the tip, while cables goes through the tip and is connected to the end of the tip as shown in Figure 3.8a. Pulling the cable result in a force in the tip and bends the tip under an angle. The outer shell of the tip works as a spring and gives a centring force as the tip is bended. Research shows a linear coupling between the tension in the conduit cable and tip angle [5]. This is verified by measurements on the TeleFLEX using a current measurement of the motor controllers.

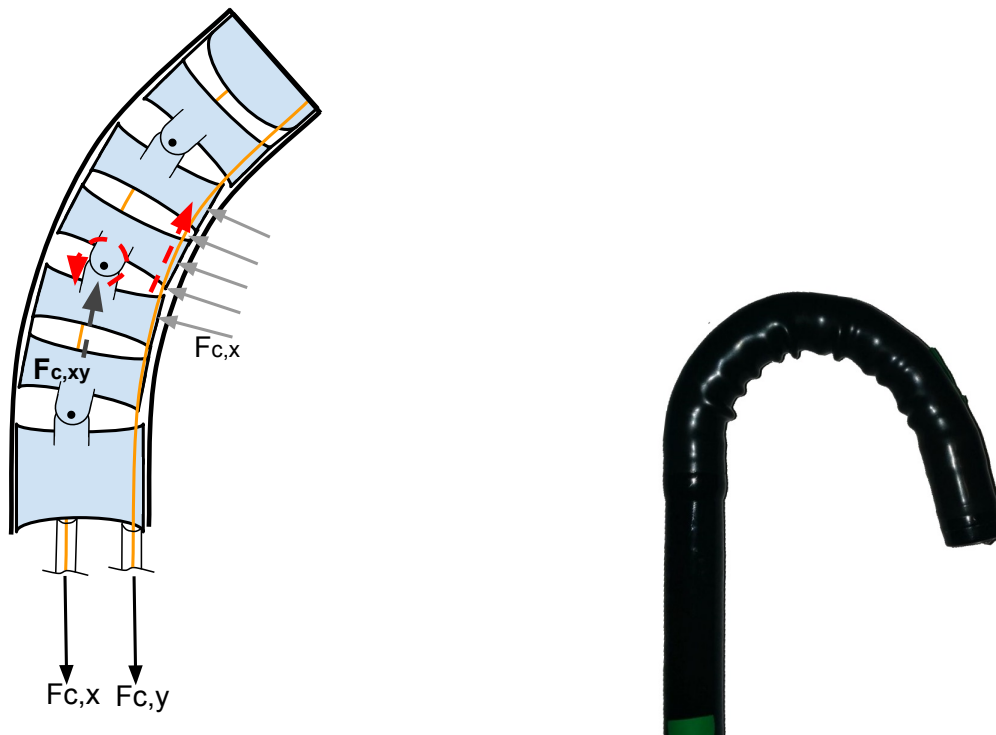
The feed forward kinematics shows that the tip position and orientation is linear, depending on the orientation angles  $\Phi_x, \Phi_y$ . This is used to model the tip friction force in the angle domain. The linear coupling between the tip angle and conduit force is done, using a rotational spring which is coupled at the end of the conduit cable over the transformation factor Equation (3.28). This gives Equation (3.31), where the  $\phi_{x,y}$  is the rotational speed of the tip in the x or y direction,  $\Phi_{x,y}$  tip position in radians in the x or y direction,  $K_{tip}$  the spring constant of the tip, and  $\tau_{tip}$  is the torque which pulls the tip to the center position.

Hysteresis is an effect of friction and stiffens. Therefore the likelihood of the tip being the source of the friction is studied.

The end of the conduit cable pulls the tip under an angle. The bending of the tip result in a normal force which pushes the cable arced in the tip. This force which pushes the cable in a arc, result in a friction force. Bending the tip further requires more force of the cable. This result in more friction as the tip is pulled under a larger angle and the tension in the cable increases.

The force of both cables has to be transferred through the tip. This results in a friction in the joints of the elements. These joints are small and are likely to have some friction force. The resulting friction force of these joints should be depending on both bending angles as the total force in the tip is depending on both conduit cables pulling. The dependency of both bending angles is also visible in Figure 3.2 where the hysteresis gets wider if second bending degree is increased.

Another possible friction force is in the outer shell which stretches while bending. This stretching results in sliding of the outer shell against the internal elements. Stretching is visible as the puckers on the insight of the tip in Figure 3.8b.



(a) The friction in the pivot points. This is a reaction force of the pulling of both conduit cables. A second problem could be the friction force as a reaction reaction of the tip being pulled under an angle.

(b) The real endoscope tip under a large angle. Shows the outer shell has some relative motion with respect to the internal spine. This is clearly visible on the puckered shell.

**Figure 3.8:** Showing the possible sources of the friction in the tip.

There are multiple sources how tip friction arises. The effects of friction in the tip are also described as clearly visible by Camarillo et al. [5], where bending the tip requires more force than loosening it. Their measurement showed a linear relation between bending of the tip and loosening force. The first attempt to model friction was based on the first hysteresis measurements, using the old set-up (Figure 2.4). This showed a wider hysteresis under larger angles of bending of the tip angle. This resulted in the coulomb friction model, where part of the friction force  $\tau_\mu$  is assumed linear depending on tip angle  $\Phi_{x,y}$ . The coulomb friction model is written to be computable optimized using  $\Phi_{x,y} \tanh(100\phi_{x,y})$ . The other part of the friction force  $\tau_\mu$  is assumed to be linear depending rotational speed of the tip  $\phi_{x,y}$ .

New hysteresis measurements using OptiTrack shown in Figure 6.5, showed the dependency of hysteresis width of both bending angles. This is used to rewrite the friction model, linear based on both bending angles of the tip ( $\Phi_x + \Phi_y$ ). The parametrization of this model showed

an extra friction force  $F_n$ , not based on both bending degrees, was needed to get a corrected hysteresis width under wide range of bending angles.

The friction and rotational spring, and conduit cable are connected using a 1 junction in bond-graph. The 1 junction, models that the velocities are equal and the forces are in equilibrium. The endoscope model should calculate the equilibrium between the conduit cable force, tip friction, and tip spring. This requires adding an extra mass in Equation (3.32) to the 1 junction, otherwise the tip center force and cable tension would calculated the tip friction. The dynamical effect of this mass is kept low by using a small mass  $m_{tip} = 0.05g$ .

$\mu_n$  is used to parametrize the linear relation between the tip orientation and friction force, and  $\mu_f$  for the friction force and tip angular velocity.  $\tau_{ctip}$  is the force from the conduit cable given in Equation (3.28).

$$\tau_\mu(\Phi_x, \Phi_y, \phi_{x,y}) = \mu_f \phi_{tip} + \mu_n \tanh(100\phi_{x,y}) |(\Phi_x(t) + \Phi_y(t) + F_n)| \quad (3.29)$$

$$\Phi_{x,y}(t) = \int_0^t \phi_{x,y}(t) dt \quad (3.30)$$

$$\tau_{Tip}(t) = \frac{\Phi_{x,y}(t)}{K_{x,y}} \quad (3.31)$$

$$P_{tip}(t) = \int_0^t \tau_m dt \quad (3.32)$$

$$\phi_{x,y}(t) = \frac{P_{tip}(t)}{m_{tip}} \quad (3.33)$$

$$\tau_m = \tau_\mu + \tau_{tip} + \tau_{ctip} \quad (3.34)$$

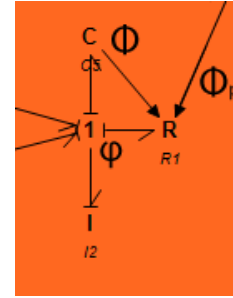


**Figure 3.9:** The 20-sim implemented the equations on the left. R is Equation (3.31), C Equation (3.31), I Equation (3.32) and 1 Equation (3.34).

### 3.2.4 The complete endoscope model

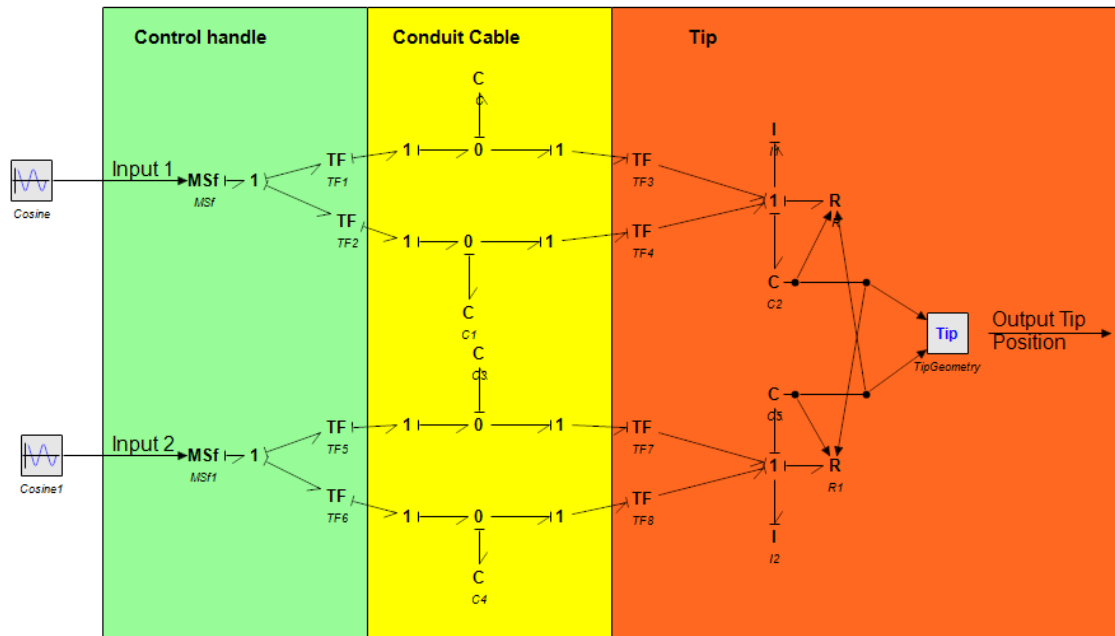


**Figure 3.10:** The 20-sim model of the endoscope. The input is the orientation velocity of the control handle. In the middle four conduit cables can be indemnified. On the right the tip dynamics is split in two and combined for calculating the forward kinematics.

The complete model is shown in Figure 3.10. This model shows two control handles on the left, four conduit cables in the middle and the tip on the right. As input a modulated source flow is used, with output being angular velocity of the control handle which is independent of the force. Two transformers simulate the control handle. The transformation ratio is depending on the internal wheel diameter which drives the conduit cable in the control handle of the endoscope as given in Equation (3.26). This is TF1, TF2, TF5 and TF6 in Figure 3.10. The conduit cable is modelled by Equation (3.5) and can only be used to pull. The model has two conduit cable pairs which are in a pull pull configuration. The change in direction of the cables pair is modelled by a difference in sign of the parameters in Equations (3.26) and (3.28). The transformation TF3, TF4 and TF7, TF8 in Figure 3.10 give the relation between the conduit cable position and tip by Equation (3.28). The tip is shown on the right. The tip forward kinematics is written in the block Tip. The output is the tip position and orientation with respect to the base. This forward kinematics is visualised using 20-sim visualisation tools in Figure 3.11.

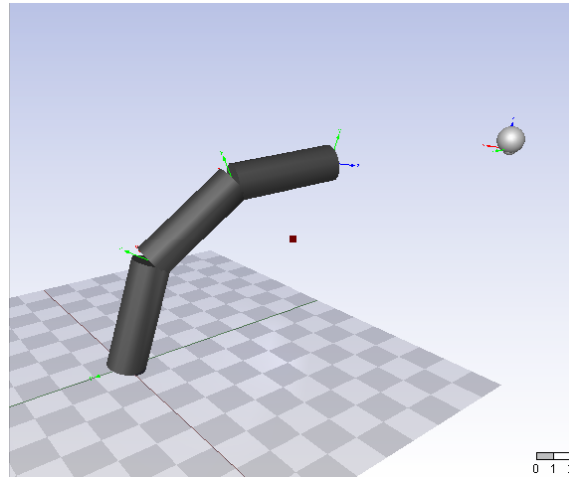


**Figure 3.11:** The tip and target visualised using 20-sim visualisation tools. The visualisation helps to validate the simulation and model.

The model is simulated using the Modulate Backward Differential Formula as integration method. First simulation results were not consistent due the internal switching of the model. Limiting the step size, showed consistent results, but made simulation slow. This is solved by adding events to the model. Events force solution of the integration when switching situation arises, for example when a conduit cable starts pulling. This made the simulation results consistent and showed the same result as using a small step-size, while keeping the simulation time within a few seconds.

### 3.3 TeleFLEX model

The TeleFLEX set-up is modelled for testing and verification of the endoscope and control algorithm. The model consists of the motor with motion controllers, the camera and the controller itself. The controller part is modelled as a discrete system, this allows to test different frame rates of the system. The motor position is sent back as feedback to the controller.

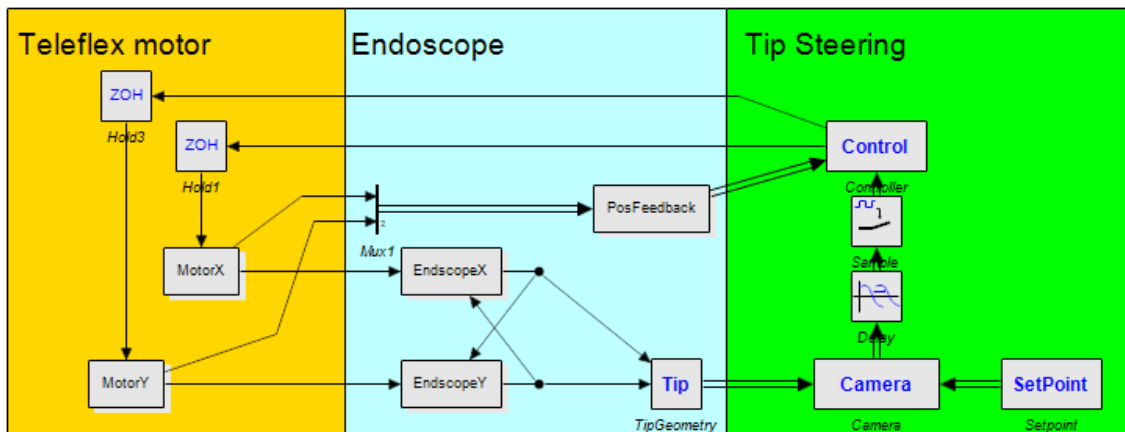


**Figure 3.12:** The complete TeleFLEX model, containing the endoscope model. Different tracking algorithms can be integrated into the control block.

The motors of the TeleFLEX are controlled in position mode, using motor controllers see Section 2.1.3. These motor controllers will prevent dynamical effects between the controller and the endoscope. This means if the motor controller is set to a position  $\Phi$ , the control handle of the endoscope will go to this position, whatever it costs. The motor controllers itself generate

a path to a setpoint with maximum velocity. The motors are modelled as a first order system, with rate limitation. The velocity of the motors is directly coupled to the endoscope control handle.

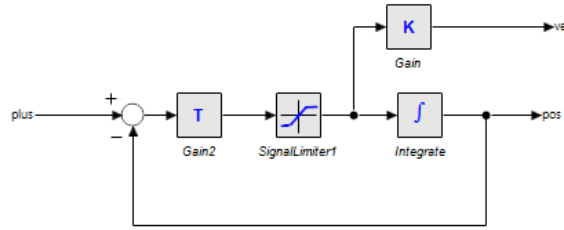


**Figure 3.13:** The model of the motor controller. The limiter limits the maximum velocity of the tip. It is first order system with rate limitation

One of the goals of this model is to test different control algorithms to track a target. The target movement is programmable so it can follow different paths. The camera is simulated, calculating the transformation matrix between the tip and target  $H_{Tip}^{Target}$ . This transformation matrix,  $H_{Tip}^{Target}$ , is transformed to pixels using the camera calibration  $K_{CameraMatrix}$  from an existing endoscope.

$$H_{Tip}^{Target} = H_{Tip}^o H_o^{Target} \quad (3.35)$$

$$P = H_{Tip}^{Target} [4, 1 : 3] \quad (3.36)$$

$$P_{Norm} = \frac{P}{P[3]} \quad (3.37)$$

$$C = K_{CameraMatrix} * P_{Norm} \quad (3.38)$$

Where

$H_{Tip}^o$ : Is the tip position from the origin.

$H_o^{Target}$ : Is the target position from the origin.

An extra latency is added to the model. The parametrization showed that latency is significant and cannot be neglected. The current vision capturing is not optimized for low latency and it assumed multiple buffers between the endoscope camera and the memory of the the vision algorithm.

### 3.4 Model parametrization

The model is parametrized to have the same behaviour as a real endoscope controlled with TeleFLEX. The parametrization can be split up in two parts: the TeleFLEX set-up driving the endoscope, and the endoscope itself.

#### 3.4.1 Endoscope parameters

The goal of the parametrization is the endoscope model having the same behaviour as a real endoscope. Some parameters could be estimated or measured using the OptiTrack and TeleFLEX set-up. These estimations and measurements are used to find the unknown parameters. Some of the relations between parameters will be explained.

The total transformation between the control handle and the tip is measured. The control handle has to be rotated 110 degrees to give the tip rotation of 90 degrees. This transformation is depending on the two transformation ratios of the endoscope and the strain of the conduit cables.

The conduit cable, controlled by the control handle, drives the tip has a stiffness of approximately 10kNm [1]. This is the stiffness of the outer conduit and internal wire in parallel.

The first transformation ratio TF1, TF2, Tf5 and TF6, is in the control handle. This links the rotation of the control handle to the translation of the conduit cables. It also transforms the conduit cable tension to torque on the control handle. The diameter should probably be somewhere between 1 and 4 cm. This parameter is fine tuned making the total transformation factor between the tip and control handle equal to the real endoscope.

The first transformation ratio gives the relation between the conduit cable linear motion and the tip rotation angle, relation is given in Section 3.2.3. Using a diameter of 12mm for an endoscope results in a transformation factor of 160[rad]/[m]. This transformation factor transforms the tip force to the force in the conduit cable. This shows, even small friction force in the tip are amplified to larger difference in tension in the conduit cable.

The friction is estimated using the hysteresis deadband plot. The hysteresis width should be equal under the different angles of the endoscope. The tip rotational stiffness should be enough to pull the conduit cable back against the friction. These parameters are depending on each other and multiple values can be found resulting in the same outcome.

The deadband is modelled as an offset in the integration Equation (3.5). This offset is transformed over the first transformation factor to the deadband angle of the control handle.

Parameter	Estimation	Simulation value	Unit
Total transformation Equation (3.2)	0.8	0.8	
Transformation 1	0.5-2.5	0.7	[cm]/[rad]
Conduit cable stiffness $K_{cable}$ Equation (3.5)	10	20	[kNm]
Deadband $L_{t_0}$ Equation (3.5)	?	0.9	[mm]
Transformation 2 Equation (3.28)	167	167	[rad]/[m]
Friction factors in Equation (3.29)			
$\mu_n$	?	0.1	
$F_n$	?	1.6	
$\mu_f$	?	0.1	
Endoscope tip rotational spring $K_{tip}$ Equation (3.29)	?	1.5	[Nm]/[rad]

**Table 3.1:** Parameters used in the model. On the left, the estimation values are given. A question mark means their was no estimated parameter available. The final used values are in the right column.

### 3.4.2 TeleFLEX parameters

The TeleFLEX uses two electro motors, driven by the Elmo motor controls. These electro motors with controllers are modelled as a first order system with rate limitation. This model results in three parameters, gain, rate limitation and time constant.

First the gain will be explained. The model of the endoscope uses radians as input of the control handle. The TeleFLEX control software uses ticks of the motor encoder to position the control handle. The gain of the first order system is used to convert the encoder ticks from the controller, to the radian angle of the endoscope control module. This allows the controller in the model, to use the same feedback gain as the real TeleFLEX set-up. The second parameter is the velocity limitation. The motion control on the TeleFLEX generates a motion path with max-

imum velocity to the setpoint. The maximum velocity is used as the rate limitation parameter. The time constant of the first order system is set to have a cut-off frequency of 10 hertz. This provides some damping from the controller which runs at 22 frames per seconds while keeping a rapid response to position changes. The real motors on the TeleFLEX also show an ideal response. This can be seen in Figure 6.5 where hysteresis compensation results in rapid changes in the measured motor position without any overshoot.

Gain	0.000016 [rad]/[ticks]
velocity limitation	100000 [ticks]/[second]
Settling time	0.2 [second]

**Table 3.2:** Parameters used for the first order system.

The latency is measured over the complete control loop. This is done by pointing the endoscope camera to the TeleFLEX control handle. The vision algorithm gives a programmed offset of the target at frame  $n$ , while recording the input. This target offset results in the auto steering algorithm to response, and steering the control handle of the TeleFLEX set-up. The steering algorithm uses a proportional controller to have an instant step response. The captured video is inspected to measure on which frame the target starts moving. Initial results showed this was after 9 frames at frame rate of 22 frames per second. This gives a delay of 0.4 second.

The tracking algorithm code is tried to be updated in order to minimize the latency. The frame capturing time is measured to check if it is from an internal buffer or extracted from the FireWire card. Frames captured from an internal buffer, take almost no time and are rejected. This is done until the capture time increases which means the frame is directly loaded from the FireWire card instead of the internal buffer. This resulted in latency of 7 frames but the frame rate is lowered to 17 frames per second, resulting around the same latency. The method is still used as it is likely the latency is more constant.

The latency is measured over the complete control loop. By inspecting the control delays, it can be shown the latency from the vision feedback. The vision algorithm integration allows the TeleFLEX software to check the vision tracking without time delays as the memory is shared. The TeleFLEX software checks the tracking algorithm at 50 Hertz. This gives a maximum latency of 0.02 seconds. Within this control step the set-point to each motor is sent, and the actual position is read out. This adds some latency but it should be within control step, it is estimated this takes a maximum of 0.1 second. The Elmo itself is hard real-time and run a control loop of 2000 Hertz resulting in a latency of 0.0005 seconds and is neglected. This makes the total latency after the vision algorithm 0.03 seconds making it likely the rest of the latency to be within the vision feedback line.

### 3.5 Model results

The endoscope hysteresis and deadband is verified by simulating the hysteresis measurement and comparing them to an existing endoscope. The model is redesigned during the project. The first model, the hysteresis was only depending on one angle of the endoscope tip. The new model, the hysteresis is calculated on both angles of the tip and static offset. Both results will be shown.

#### 3.5.1 First result

The initial model Equation (3.29) should be replaced with:

$$\tau_{\mu}(\Phi_{x,y}\phi_{x,y}) = \mu_f \phi_{tip} + \mu_n \tanh(100\phi_{x,y})|(\Phi_{x,y}(t))| \quad (3.39)$$

The result of the first model shows the hysteresis get wider under larger angle of the endoscope tip. This initial friction model is used as a base for the hysteresis compensation width.

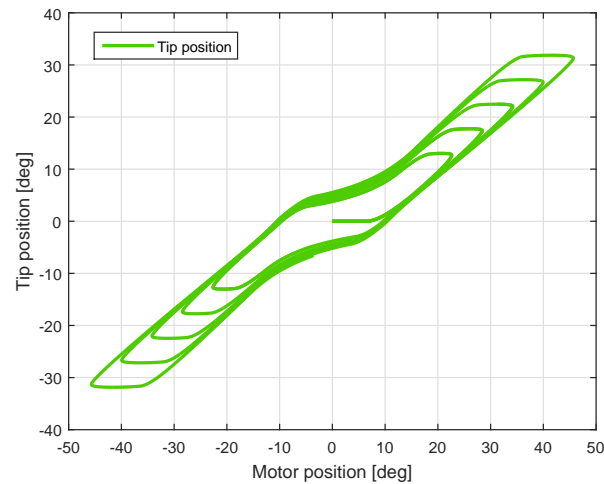


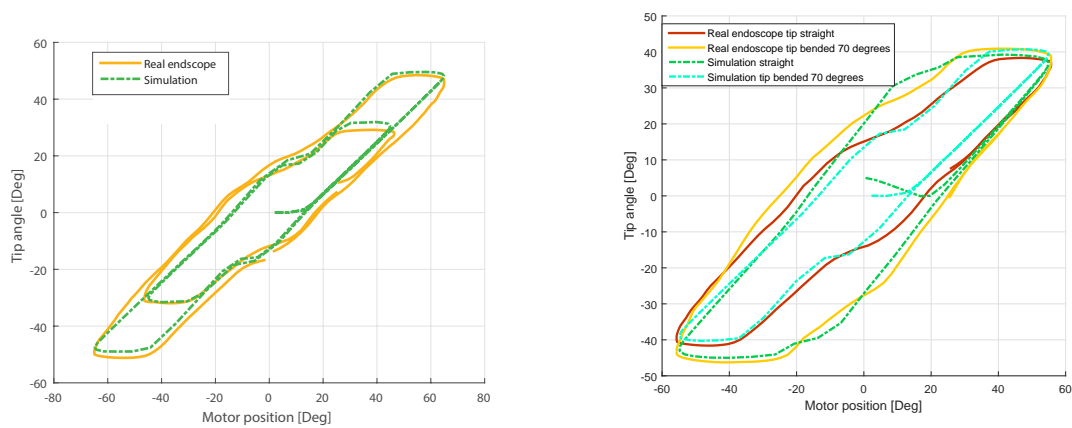
**Figure 3.14:** The hysteresis curve of the first model

### 3.5.2 New result

During the validation of the hysteresis compensation, it became clear it did not work as expected. The hysteresis compensation only showed result under larger angles of the tip. This resulted in the new hysteresis measurement with the OptiTrack as described in Section 3.1. The parametrization of these values resulted in a new friction model Equation (3.29). The hysteresis and deadband of this new model are verified by comparing hysteresis measurements of a real endoscope with the OptiTrack systems to the model simulation.

The first verification shows the tip bending under small and larger angles, while second bending angle of the tip is straight. The result shows the model hysteresis width is quite accurately compared to the measurements of a real endoscope. The real measurements show, the hysteresis width stays constant in the returning path of the endoscope tip to the center. In the model the friction force is calculated based on the tip orientation. This means the hysteresis width in the model does not stay constant on the returning path to the center, and get even slightly smaller.

The real set-up measures, showed the deadband entering is depended on the maximum angle of the tip. The entering of the deadband is an equilibrium between the endoscope friction and tip centring force. The tip enters the deadband and stops moving if the tip friction is larger compared to the centring force of the tip. The entering of the deadband would be correctly modelled, if the friction force stayed constant after the tip switching direction to the center direction of the tip.



(a) Tip orientation is rotated around degree of freedom while the second tip angle set constant angle of 0 degrees. The dashed line are the simulation.

(b) Tip orientation is rotated around degree of freedom while the second tip angle is set constant of 70 degrees. The dashed line are the simulation.

**Figure 3.15:** The hysteresis validated by comparing the 20-sim simulation with the OptiTrack hysteresis measurements.

The second verification shows the bending of the tip around one of its axis, while the second axis is set to zero and 70 degrees. The model and real endoscope show a wider hysteresis when tip is bended in both degrees. The model also shows the deadband is entered earlier when the tip is bended under the second angle.

The deadband can be changed, this shows similar behaviour found with earlier measurement before the endoscopes was calibrated Figure 2.4. This is an imported feature as the deadband changes between endoscopes or when the endoscope is bended.

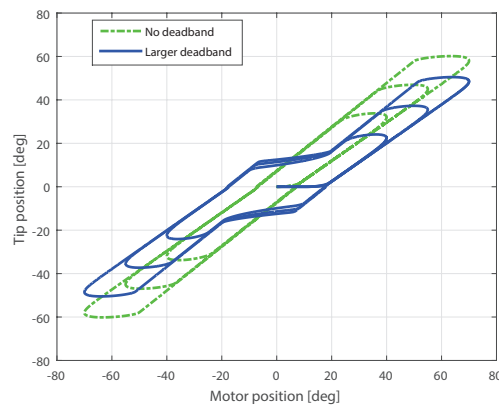


**Figure 3.16:** In simulation the tip is bended under one degree of freedom while second tip angle is kept zero. It shows the model has similar behaviour if the deadband is changed.

### 3.6 Summery

In the beginning of the project, the hysteresis and deadband measurements, as shown in Figure 2.4, where available. These measurements showed the effects of hysteresis and deadband between the endoscope control handle and tip. The real cause of hysteresis and deadband was unknown. In the first part of this project the hysteresis measurements were coupled to the motion of the tip and conduit cables in the endoscope shaft. This showed why the deadband always appeared around the tip center position. The tip centring force keeps one conduit cable

tensioned during the bending. The deadband is entered if the friction force is larger compared to the centring force of the tip.

The hysteresis is a more complex effect. The chapter 3 describes multiple sources of friction in bending of the tip. The model results show that hysteresis can be modelled quite accurately using the friction in the tip and the stiffness of the conduit cables. The model contains a simplified friction model, this causes the hysteresis width not to be completely correct on the returning path of the tip to the center, and entering of the deadband.

The modelling and parametrization of the TeleFLEX set-up showed latency as a real issue. Latency is going to limit the performance of the target lock.

---

## 4 Control design and implementation

The aim of the project is to implement auto steering for the tip of an endoscope. The auto steering algorithm uses the vision algorithm as input for steering the tip to keep it focused on a target. The vision algorithm is designed to track a point in the image. Three different control algorithms are designed, tested in a simulation, and integrated on the TeleFLEX set-up.

Previous research by Ott et al. is done for developing a tracking algorithm using the camera of the endoscope as feedback [10]. They choose a different approach due to different conditions. Their goal was to stop motion between the camera and a mechanical ventilated patient. The ventilation resulted in a periodical movement of the target with respect to the camera. This assumption can not be made in endoscopy. Breathing has no influence in the movement in the gastrointestinal tract. Their feedback control loop used the vision algorithm to extract the optical flow of the camera. The optical flow is translated to joint velocity of the tip using the geometric Jacobian. This is combined with a controller optimised for periodical motion. The hysteresis and deadband of the endoscope tip resulted in larger errors of the tracked targets. This was solved by online hysteresis and deadband estimation, using the vision algorithm to measure the tracking error due to hysteresis and deadband. This was only possible because the target position was known due to its periodical movement. Hysteresis and deadband measurement was injected in the feedback. This approach is not usable when investigating the gastrointestinal track because the periodical motion is non-existing.

Our approach is based on using the vision algorithm to robustly track one point on the target. This is used as feedback to steer the tip. This approach allows the hysteresis and deadband to be controlled using purely the feedback. Hysteresis and deadband have a negative influence on the control loop and will result in large tracking error. This can be solved using active hysteresis compensation which is injected in the feedback.

### 4.1 Vision algorithm integration

The vision software uses the functionalities of OpenCV. OpenCV is a library combining multiple packages for images. Each package in OpenCV has multiple interfaces to the different languages like C, C++ and Python. Not all of the packages have interfaces to all of the different programming languages. The vision algorithm uses the OCL package of the OpenCV library to integrate OpenCL. OpenCL is a standardized interface allowing calculation for heterogeneous platforms, the tracking algorithm uses a Graphics card. The OpenCL accelerates the vision algorithm, and allows it to run at a frame rate of 24fps. The OCL package of OpenCv has interfaces designed for C++ or C. This means the existing vision algorithm cannot be programmed in Python, as the rest of the TeleFLEX software. Another advantage of C++ that it is faster than Python, this gives more space for complex operation, as filtering.

The TeleFLEX software, written in Python, needs to communicate with the vision algorithm written in C++. The main goal of the integration, it has to be fast, reliable and easy to use. The old implementation used socket connections to connect the TeleFLEX with the vision algorithm. This implementation was limited integrated in the current TeleFLEX software. Due to lack of documentation this implementation is not tested.

A new implementation is designed by adding a Python interface to the vision algorithm, making it a native Python Extension. This allows the Python code to directly communicate with the vision code using shared memory. This is a fast and reliable connection compared to using sockets. The vision algorithm itself is driven in a different thread, using windows API. This allows it to run parallel with the Python code. The Python integration allows the tracking algorithm to be started directly from the current software. The TeleFLEX software has a control

loop, running at 50 hertz used for the different steering modules as described in Section 2.1.4. This control loop is extended with the new control algorithms. The auto steering is added as a separate tab in the current TeleFLEX GUI as shows in Section 4.1. The GUI is also used to quickly change parameters of the control algorithm and different features of the tracking algorithm.

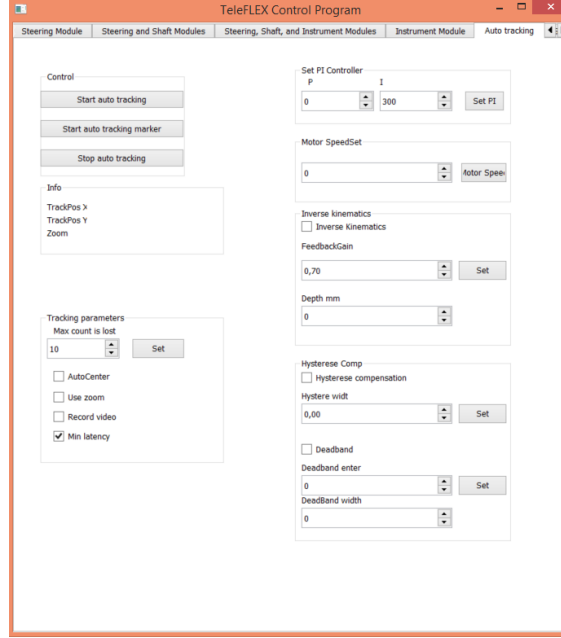


**Figure 4.1:** The target lock is completely integrated in the current TeleFLEX software.

## 4.2 PI control algorithm with hysteresis suppression design

The  $I$  controller is already used with the lumen steering on the TeleFLEX set-up [15]. This simple controller can be used, as the conduit cables steering the tip, are statically mounted to the camera frame. These cables are aligned with the camera  $x$  and  $y$  direction in pixels. This allows the offset from the target in pixels to be directly used as feedback to steer the tip. The target position in the image is translated to be relative to the center of the image. This allows the target position being directly used as feedback. The target offset is controlled to zero. The final design used only the  $I$  action of the PI controller. The  $I$  action moves the tip in the direction of the target offset, from the center. The  $P$  action couples part of the offset in pixel directly back to the motor position, it is implemented, but currently not used, to make the hysteresis compensation more predictable.

The  $\Phi$ ,  $X$  and  $Y$  bending direction are controlled separately based on the offset in the  $x$  and  $y$  directions in the camera image. The discrete mathematical expression for controlling the bending direction of the tip  $\Phi_x$  direction is given in Equation (4.2).  $x$  is the offset of the target with respect to the center,  $S\Phi_x$  is the motor setpoint and  $dt$  is the time step size. The  $y$  direction can be expressed by substituting  $y$  for  $x$

$$L_{x,n} = L_{x,(n-1)} + x_n \quad (4.1)$$

$$S\Phi_{x,n} = IL_{x,n}dt + Px_n \quad (4.2)$$

$$(4.3)$$

The initial output value of the controller should avoid the tip from moving. This is done by setting the integrating state  $L_{x,n}$  equal to the tip orientation  $\Phi_x$  on initialization of the target lock.

### 4.2.1 Distance influence

The camera of the endoscope uses a lens to project the target on the sensor plane. This projection causes the measured offset to increase, when the target is brought closer to the camera. The PI controller bends the tip to bring the target back in the center of the image. The amount the tip has to bend to get the target back in the center, is depending on the measured offset and distance of the target.

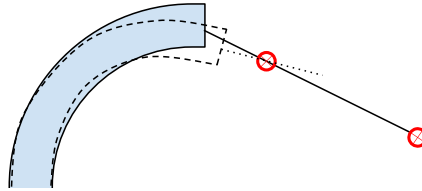


**Figure 4.2:** Both targets are seen on the same spot in the image due to the lens and the projection. The tip has to rotate further, to get the furthest target in the center of the image.

This means, the PI controller parameters are depending on the distance between the camera and target. The PI parameters are currently estimated using the experimental design Section 5.2. The found parameters are only valid for the used distance.

### 4.2.2 Hysteresis compensation

Hysteresis and latency limits the performance of the PI controller. The  $I$  action can be used to control the final error due to hysteresis. This requires a high integral parameter what is not possible due to latency in the control loop. Hysteresis compensation should help the PI control to keep the target in the center. The hysteresis compensation does not have to be perfect, as the integral controller will ensure that the final error becomes zero. The hysteresis compensation is added the steering setpoint.

The current integrated design is based on the first model in Section 3.5 and the endoscope lying straight. The endoscope is recalibrated during the project, this minimised the deadband of the endoscopes. Experiments showed the deadband was too small to be effectively compensated. This can be seen in the hysteresis measurement in Figure 3.2 where the deadband does not result in a horizontal section in the center as can be seen in the earlier measurements in Figure 2.4a. In the current hysteresis compensation deadband is not taken into account.

Hysteresis is a problem when the endoscope tip switches direction as can be seen in the measurements. The model shows this can be explained due to friction in the tip and stiffness of the conduit cables. The change of direction is used for the switching conditions of the algorithm. The hysteresis measurement showed the hysteresis width is depending on angle of the tip. The measurement also showed hysteresis stays the same width after switching direction. The hysteresis compensation is switched on, when steering setpoint switches direction to the center of the tip. The hysteresis compensation is reset to zero when the tip steering setpoint direction, is switched again. The switching is only allowed if the target is more than 10 pixels out of the center, this prevents rapid switching if the target is nearly in the center.

The  $w$  parameter gives the linear relation between bending of the tip and hysteresis width. The linear relation between the hysteresis width and bending results from the hysteresis measurements and the modelling phase. This parameter needs to be measured for each endoscope. This could be done by using the old or new hysteresis measurement set-up. Current experiments are conducted by maximizing the hysteresis compensation resulting in a slightly over-estimated width. The tip bending angle is currently set equal to the measured motor position  $M\Phi_x$ .

$$D = \text{sign}(\Phi_{(x,n)} - \Phi_{x(n-1)}) \quad (4.4)$$

$$H = \begin{cases} H = 0 & \text{if } D = D \text{ and } |x| > 10 \\ H = M\Phi_x w & \text{if } -D \neq m \text{ and } H \neq 0 \text{ and } |x| > 10 \end{cases} \quad (4.5)$$

The initial design was based on combination with deadband compensation around the center position. The deadband compensation was subtracted from the hysteresis, and hysteresis was set to zero. The recalibration of the endoscopes made deadband compensation useless, this means the hysteresis switching conditions needs to be redesigned to work correctly around the center of the tip.

### 4.2.3 Control overview

The complete control loop is given in Figure 4.3. The vision algorithm tracks the target with respect to the center of the image and gives the offset  $x, y$ . The PI controller is given in Equation (4.2). The hysteresis compensation uses the control signal for switching conditions, and the actual motor position for calculating the hysteresis width.

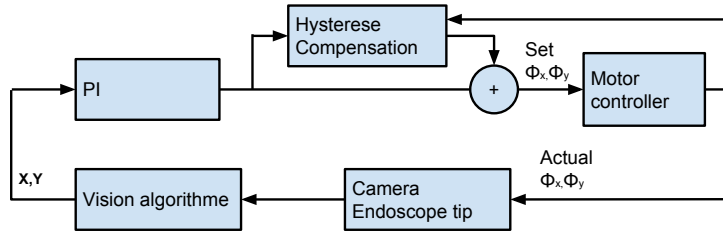


**Figure 4.3:** The PI controller with hysteresis compensation control loop. The hysteresis compensation can be switched off.

### 4.3 Inverse kinematics design

The PI controller steers the tip without any knowledge of the forward kinematics of the tip. The inverse kinematics control algorithm is based on calculating the joint position setpoint, to get the target in the center of the camera again as shown in Figure 4.4. Inverse kinematics makes the feedback more precise, resulting in a more responsive system. The influence of depth between the target and camera, can also taken into account, using the inverse kinematics control algorithm.

The second advantage of the inverse kinematic is that it deals better with latency. For example, a step response of the target, results the PI controller to keep integrating during the latency, potentially overshooting the target. The inverse kinematics calculates a constant setpoint during the latency steering the tip to the target.

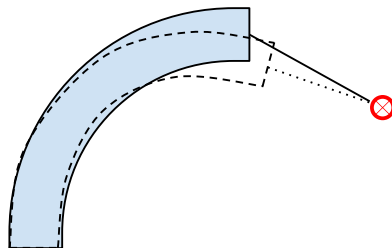


**Figure 4.4:** In the first control step, the tip angle and target are measured, this is used to calculate the setpoint to get the target back in focus, as given as the dotted line.

The first step of the designed inverse kinematic control, is calculating the target position with respect to the camera in 3D. The model of the TeleFLEX set-up already showed how a 3D position can be projected to the offset in 2D on the image plane using the camera matrix. Equation (3.38) is inverted to calculate the 3D position of the target with respect to the camera frame, using the measured offset in the image plane. This requires the distance between the target and camera frame. Currently the static measured distance between the target and camera is used. The initial idea was to use the zooming factor of the tracking algorithm. This was impossible as the zooming factor did not work correctly.

The second step is to calculate the new setpoint of the tip bending so the target is focused again. The forward kinematics is written by changing the degrees of freedom Equation (3.20). This solution does not allow to derive mathematical inverse of the forward kinematics. This is solved by using the model of the endoscope and TeleFLEX in an online simulation for each control step. The model simulates the tip orientation so the target is focused again.

The online simulation requires the setpoint with respect to the base, instead of the camera frame. The target position, expressed with respect to the camera, is translated to the base using the feed forward kinematics (Equation (3.20)) of the tip. The forward kinematics of the tip is coupled to the motor position of the TeleFLEX set-up. The model used for the online simulation is simplified to only the forward kinematics, motors and PI controller. The simplification is needed simulated during the control.

For each control step, the target position with respect to the camera, is measured using the tracking algorithm. The target position is translated to a 3D position, using the camera matrix and depth estimations. This position is translated to the base of the endoscope tip, using the forward kinematics of the tip. This is used as setpoint for the simulation. The simulation uses a simplified model to simulate the tip orientation to get the target in the center of the image. The final value of the orientation in simulation, is used as setpoint for the real controller. New setpoints are only calculated when new tracking information is available.

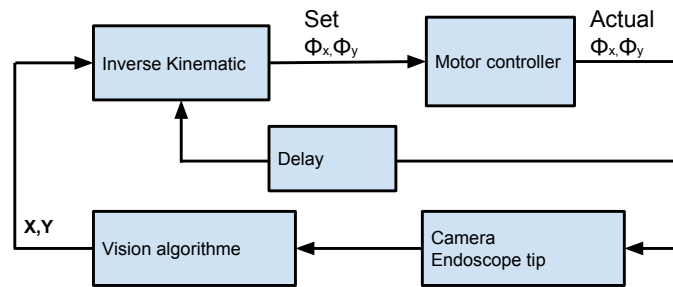


**Figure 4.5:** The inverse kinematic control loop. The inverse kinematic block is visualised in Figure 4.7

The inverse controller, as shown in Figure 4.5, shows a delay line on the motor position feedback. This was necessary as the camera has a latency of around 0.4 seconds while the motor position feedback is almost zero. The control algorithm delays the motor position with 8 frames to synchronize it with the camera image. Without this synchronization, the controller is unstable. The synchronization between the camera image and the setpoint generation is not completely accurate. This is solved by adding damping  $d$  between the generated setpoint  $S\Phi_x$  and the actual motor position  $M\Phi_x$ .  $d$  is set to 0.7, this keeps the controller stable, and simulation showed it has minimal impact on the controller performance.

$$S\Phi_x = S\Phi_x - d(S\Phi_x - M\Phi_x) \quad (4.6)$$

The current implementation of the inverse kinematic controller, does not take hysteresis and deadband of the endoscope into account. This is tried using the feed-forward control of the PI controller in Section 4.2.2 for suppressing the hysteresis. This did not have the desired effect. The inverse kinematic controller used the actual motor position for calculating the setpoint for the simulation. The feed forwarding hysteresis suppression, results in large steps in the motor position. These large steps give probably some unwanted effects in calculating the setpoint, using the inverse kinematics.

The tip forward kinematics is calculated using the motor position on the TeleFLEX set-up. This means the deadband and hysteresis results, in the simulated forward kinematics model, are not in complete synchronisation with the real endoscope tip, as shown in Figure 4.6. Despite the tip orientation is not completely correct in simulation, the feedback to get the target back in focus again should be quite correct. The tip behaviour only changes slowly over the working area of the tip bending.

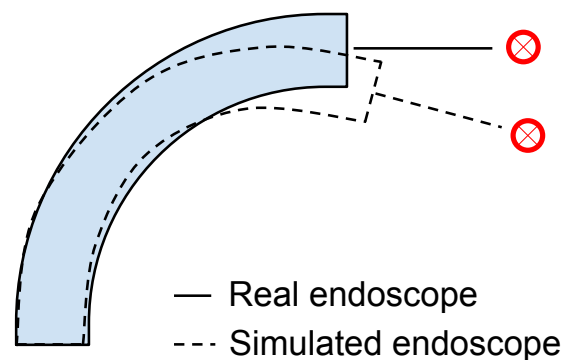


**Figure 4.6:** The hysteresis and deadband results of the simulated tip orientation, is not complete synchronisation with the real endoscope tip.

#### 4.3.1 Inverse kinematic technical implementation

The online simulation of the model required some software implementation to the current TeleFLEX software. 20-sim has code generation, allowing the model with integration algorithm, to be exported to C-code. The generated C-code is integrated into the TeleFLEX software, by adding a Python interface as the tracking algorithm Section 4.1. The generated code itself, is also tested in simulation. This is possible because 20-sim allows the use of external C-code during simulation. This required a second interface for the generated 20-sim code.

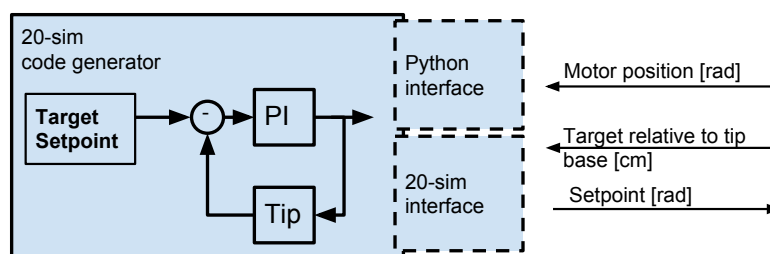


**Figure 4.7:** Overview of parameters that needed to be estimated.

The simulation uses discrete integration method with a optimised step size to make the exported code fast enough to be run during the control. Tests showed the simulation time was approximately 0.001 second which is within the control loop that runs at 50 hertz.

## 5 Experimental design

The experiments are designed to test and compare the different tracking algorithm, and verify the tracking algorithm is working correctly. The results of the experiments are also used to validate the model in Chapter 3 of the TeleFLEX and endoscope. During the experiments, the OptiTrack is also used to track the target and endoscope. The OptiTrack is used to validate the vision algorithm is working correctly during the experiments [17].

### 5.1 Target design

A special target to test auto tracking and auto steering is designed. The target is optimized for the vision auto tracking algorithm. An image of the inside of a colon is taken with an endoscope and is printed on A4 paper. The image was maximized on the A4, to not negatively influence the auto tracking algorithm. The lighting of the target needed to be optimal for correct working of the auto tracking algorithm. The endoscope has its own light source. Tests showed this could not be used due to reflection of the paper. Powerful floodlights did work for the auto tracking algorithm, but the OptiTrack balls could not be detected because of the floodlight. The solution was to use a led strip on a plate behind a Plexiglas plate. The printed target is put on Plexiglas, and is lighted from behind as shown in Figure 5.1.

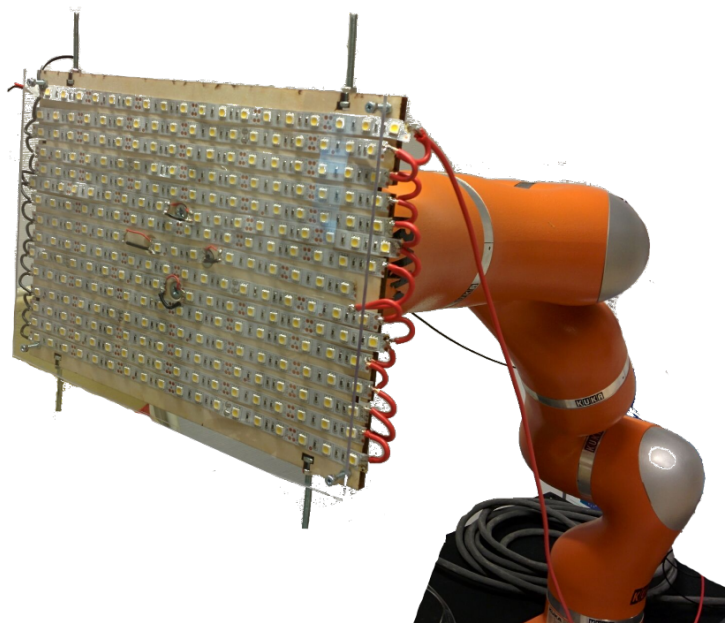


**Figure 5.1:** The target mounted on a KUKA robotic arm. The led strip is mounted behind the Plexiglas plate.

During the initial testing phase, it became clear that blurring due to motion of the camera could not be prevented completely. The vision algorithm stopped when the target could not be detected in the new frame. This is not ideal when verifying the target lock. Therefore the tracking algorithm is adjusted to neglect frames that could not find the selected target, as shown in Figure 2.6. This resulted in a robust image algorithm, usable for the experiments.

For the next experiments the vision tracking algorithm is assumed to be correctly tracking one point on the target.

## 5.2 PI parameter estimation

The PI controller needs to have a I parameter to work correctly. The I value is determined using a step response on the TeleFLEX set-up. This is done on the TeleFLEX using an endoscope to insure all the dynamical behaviour due to non linearity from the hysteresis and deadband, are taken into account.

To get the step response, the tip is set in straight known position, with the target described in Section 5.1 in front of the camera. The tracking algorithm is adapted to select the target at one quarter of the width and half the height of the camera image. This results in a step response of the target lock. Different parameters can be compared by resetting the tip to its original state, and reselecting the target. This experiment should be redone if the distance between the camera and tip significantly changes as shown in Section 4.2.1.

## 5.3 Controller performance verification

The aim of the project is to design a target lock for endoscopes using the TeleFLEX set-up. The three designed auto steering algorithms: PI control, PI control and hysteresis compensation, and inverse kinematics control, can all steer the tip to keep the target focussed. This is tested by moving the endoscope or target by hand, and looking at the image of the camera. This shows the target is almost not moving while the endoscope or target is moved. The designed experiments are mainly focused on measuring the difference in performance between the three designed control algorithms. A good performing tracking algorithm should steer the tip to keep the target focussed in the center of the image plane. Any offset of the target from the center is called the tracking error.

The target, as described in the previous Section 5.1, is mounted on a KUKA robotic arm as shown in Figure 5.1. The robotic arm can move the target in a periodic, and highly repeatable way. This allows different control strategies to be tested, with minimal changes of the target movement. The robot path is programmed using the standard software of the KUKA arm. The KUKA software allows setpoints to be programmed by moving the the robotic arm by hand. The actual distances of the path are measured using the OptiTrack.

The target selection of the vision algorithm is changed to make the testing of different control algorithms more consistent. Target is automatically selected in the middle, with constant size instead of the user selecting a target.

The robotic arm is programme using two different paths. The first path consists of moving a target straight over a distance of 12cm with a frequency of 0.1 Hertz as shown in Figure 5.2a. The distance between the tip and target is not constant due to motion of the tip and target. Their is a 1 second stop between each full linear motion. The second path consists of moving the target in a circular motion as shown in Figure 5.2. The final programmed path is an eclipse with from top to bottom 12cm and left to right 13cm. The rotational frequency of the target is around 0.05 hertz. The circle motion could not be programmed continuously, it contains two stops during one circular motion.

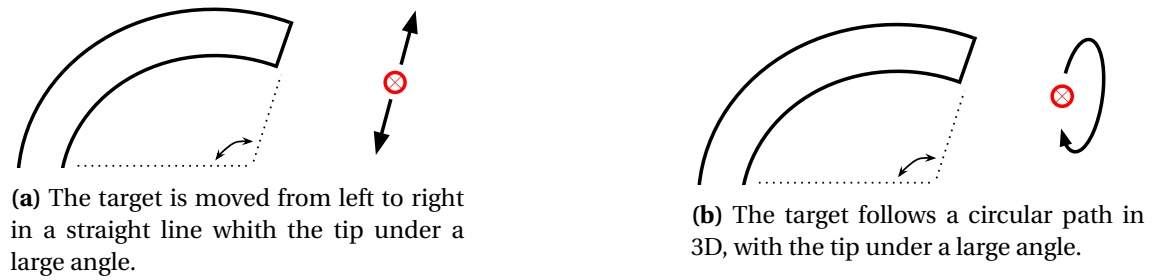


**Figure 5.2:** Path used to test different tracking algorithms.

The distance between the tip and target is set to 12 cm. This distance is a result of the large printed target that needs to be robustly tracked by the vision algorithm. The larger distance between the tip and target is compensated, by making the movement of the robotic arm bigger to make the tip move to track the target. The endoscope itself is laid straight on the table and is static mounted using tape. The different control algorithms are all tested in sequence, minimizing the effects of small differences between the experiments.

The two programmed paths of the target, are tested under different angles of the tip. These results showed, hysteresis compensation was only working correctly under larger angles of the tip. This led to new measurement with the OptiTrack and redesign of the friction model. The friction model insinuate the hysteresis width compensation should be depending on both bending degrees, and a constant value. This new hysteresis compensation is currently not integrated and tested on the TeleFLEX set-up. The experiment results using the old hysteresis compensation, are presented. These results show, hysteresis compensation can have the desired effect on the target lock.

The result of these experiments are also compared to the simulation results to verify the model of the TeleFLEX and endoscope given in Chapter 3. This is only performed on the straight target path, as the circular path with its stops, is difficult to get correctly programmed in the 20-sim simulation.

## 6 Experiment results

### 6.1 PI parameters

First the  $I$  parameter of the PI controller is estimated using experiments as described in the previous chapter Section 5.2. The result in Figure 6.1 show the step response for different  $I$  parameters of the PI controller.

A low  $I$  action result in a slow response, while a higher  $I$  action contains more overshoot. The highest  $I$  value showed, some frames were occasionally dropped due to high velocity of the tip camera. The finale value of 300 for  $I$  is used to compare different tracking algorithms and simulation. This response has some overshoot, leaving space for suppressing hysteresis using purely feedback.

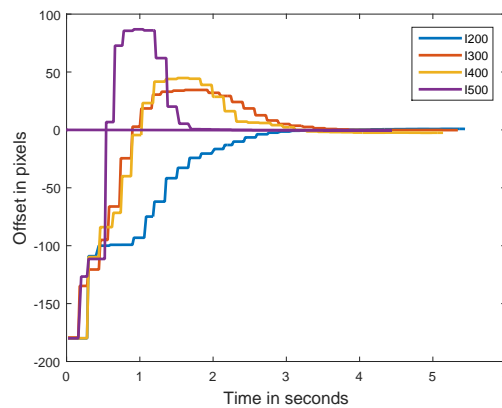


**Figure 6.1:** The response for different  $I$  parameters are shown in one plot. At  $t_0$  the target is selected at  $1/4$  of the image width. This results in the tracking error of -180 pixels. The target lock responds and steers the tip to get the target in the center. The blocking is due to the frame rate of the vision algorithm.

### 6.2 Target lock and model validation

The first results are shown in Figure 6.2. The target is moved linear and hysteresis compensation is on. The target lock rotates the TeleFLEX motors between 20 and 60 degrees to keep the camera focused on the target. The target stays within 150 pixels of the image center. This shows the target lock is working correctly. More information on the tracking error will be given in the next section.

The results in Figure 6.2 are mainly presented as it shows the periodical, dynamical response of the target lock. This is a result of the periodical motion of the target. The constant periodical dynamic behaviour is used to compare the different tracking algorithms, and simulation with the experiments. The next analysis given in this chapter will only show two linear motions of the target path.

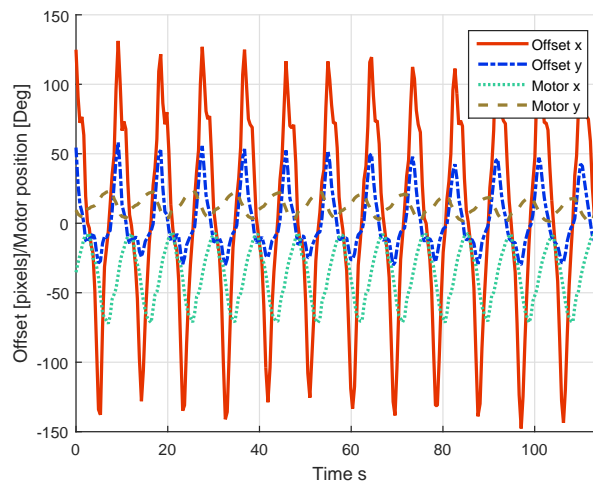
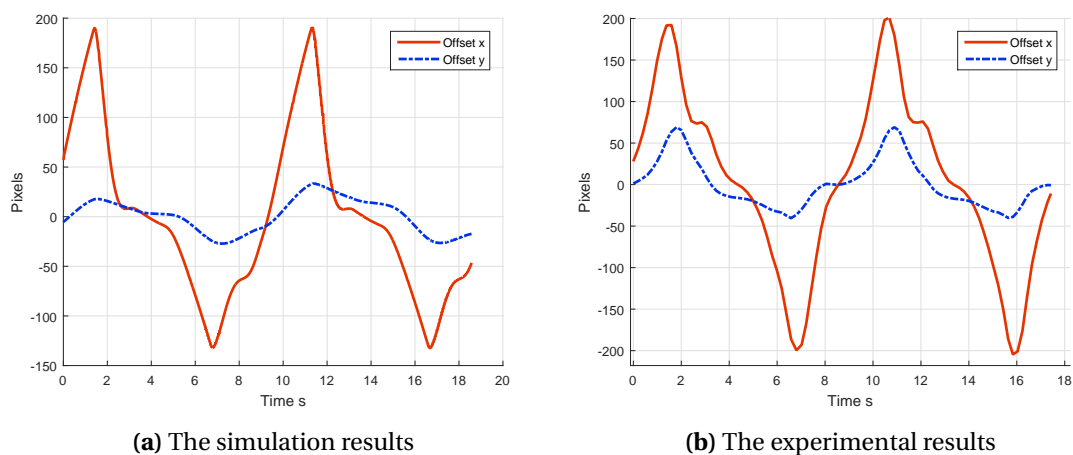


**Figure 6.2:** The plot shows the tracking error of the target, and motor position of the TeleFLEX in degrees, are plotted in time. The target is linearly moved with a frequency of 0.1 Hertz. This is clearly visible in the tracking error, peaking at the same frequency. The motor position, given in degrees, also shows the same periodical frequency.

The complete model of the endoscope and TeleFLEX set-up as given in Chapter 3 is verified by comparing the PI controller performance in simulation to the real situation. The linear motion of the target is used, and the tip is under a maximum angle of  $-80$  degrees. The tracking error is split in x and y direction for the simulation and experiment.

The programmed target path in simulation is done to be as accurate as possible. The simulation uses a feedback parameter of 310 for  $I$ , this gave a more comparable dynamical result. The small difference in gain can be explained by an error in the gain of the motor in the simulation, see in Section 3.4.2.



(a) The simulation results

(b) The experimental results

**Figure 6.3:** The tracking error in the x and y direction of the target. A perfectly focused target appears as 0. The tip is moving to keep the target focused.

The dynamical behaviour of the model simulation, is similar to the real situation. The effects of hysteresis for full tracking cycle in simulation and experiment is given in table 6.1.

Time	Tip angle	Action
4 Seconds	-10 Degrees	The target starts moving and the tip is not responding due to hysteresis. This increases the tracking error.
7 Seconds	-10 Degrees	The control handle is rotated enough for the tip to respond again. This lowers the tracking error to zero.
9 Seconds	-70 Degrees	The target switches direction and the tip stops responding due to hysteresis. The tracking error starts to increase.
11 Seconds	-70 Degrees	The tip starts responding and the tracking errors starts to decrease.
12 Seconds	-10 Degrees	The target is stopped for 1 second. This results in a small flat plateau.
14 Seconds	-10 Degrees	The target starts moving again and the same periodical response starts again at 4 seconds.

**Table 6.1:** An overview of the dynamical effects in Figure 6.8.

In Figure 6.8 can be seen, both direction having a small tracking error. The OptiTrack showed the target was actually not completely moving in one line, but in a narrow ellipse. This is probably an effect of programming the robotic arm by hand. This target path is also programmed in the simulation.

The experiments shows peaks in the y direction of 200 pixels positive and negative. The model shows peaks of 190 pixels and -140 pixel. The difference between positive and negative tracking error in the simulation can be explained. The model does not have the dynamical behaviour, with the hysteresis width staying the same size on the path of the tip returning to the center as shown in Section 3.5. This results in less hysteresis if the target direction is switched under smaller angles of the endoscope tip in the simulation.

The model is also used to check how tracking is performing, using zero latency. This result is almost an identical plot with tracking error peaks approximately 40 pixel smaller. This confirms hysteresis is currently the main source for the target tracking error, and latency should be taken into account.

### 6.3 Different tracking algorithm performances

Different control strategies are designed and integrated on the TeleFLEX set-up as described in Chapter 4. The performance of the different control strategies are compared, using two paths of the target as given in Figure 5.2. The tracking results of the simulation are also compared to the real TeleFLEX set-up. This shows the applicability of model to predict the improvement in control using a new control strategy.

First, the PI controller with hysteresis compensation, is compared to the PI controller. The hysteresis compensation width, Equation (4.5)  $w$ , is set to 0.2 in simulation and the TeleFLEX set-up. The tracking error the x and y direction is summed using Pythagoras to the total tracking error from the center. The target is moved in a straight path.

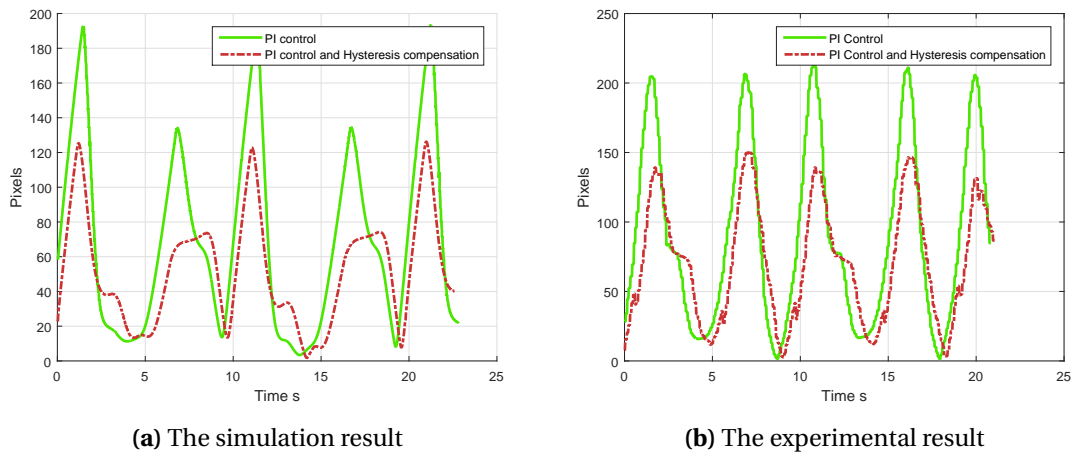


**Figure 6.4:** The plots show tracking error of the target, while the target is moving in a linear motion. The PI controller is compared to the PI controller with hysteresis compensation.

The simulation shows two difference peaks of the tracking error, compared to the experiments. This is again because of the unmodeled behaviour, of hysteresis not staying the same width on the returning path to the center. Hysteresis compensation is designed for the hysteresis width staying the same. This result in larger hysteresis compensation around 8 and 18 seconds in the simulation.

The experiment and simulation show that the target stays around 65 pixels closer to the center using the hysteresis compensation. The experimental result shows the hysteresis compensation is slightly overestimated. This can be seen in Figure 6.4b where a small discontinuity in tracking error at 1,6,10,15 and 18 second. The simulation does not have these discontinuities, but hysteresis overestimated compensation in simulation results in the same effect as the real set-up, unstable behaviour.

The hysteresis compensation can clearly be seen, by plotting the measured motor position and tracking error of the target Figure 6.5. This shows the control handle is rapidly changing direction with minimum change of the target with respect to the center.

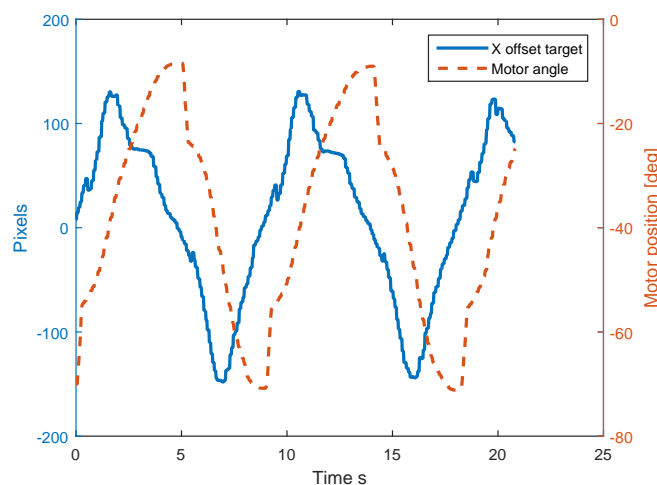
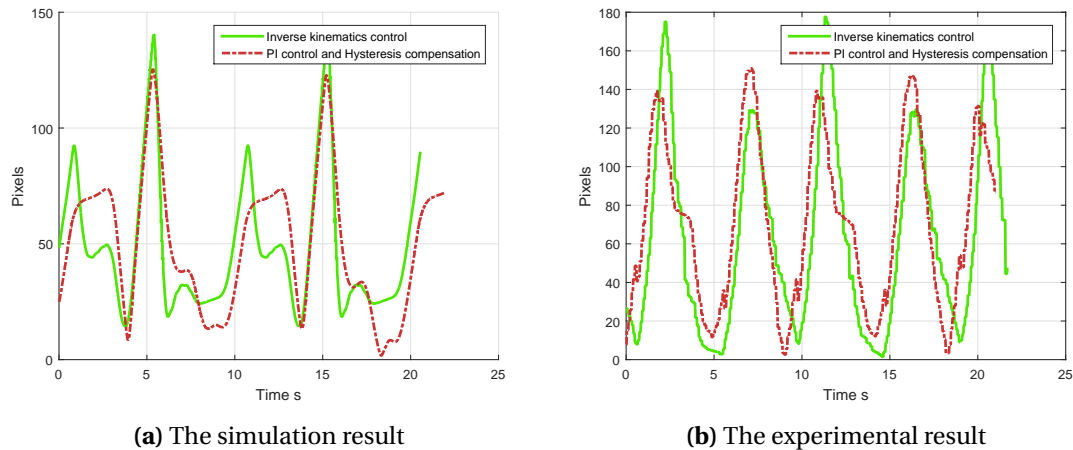


**Figure 6.5:** The tracking error and motor position in the X direction. The steps in the motor position are the hysteresis compensation.

Next the inverse kinematic controller is compared to the PI controller with hysteresis compensation. The straight path of the target is used again. The distance between the target and tip for the inverse kinematic control algorithm is set to 12cm, this is the initial distance measured. Due to motion of the tip and target, this distance increases to 16cm if the target is furthest away.



(a) The simulation result

(b) The experimental result

**Figure 6.6:** The plots show tracking error of the target, while the target is moving in a linear motion. The inverse control algorithm is compared to the PI controller with hysteresis compensation.

The model shows small improvements using the inverse kinematic model, compared to the PI controller with hysteresis compensation. This is expected as the simulation uses the same forward kinematic model for simulating the tip and predicting the setpoint, making it more accurate compared to the experiment. The experiment shows the inverse kinematic controller performance comparable to the PI control with and without hysteresis compensation. The experiment's inverse controller shows different peak tracking errors when the target switches direction. This is likely to be an effect of the distance which is assumed to be static in the inverse kinematics, while the real distance between the camera and target changes due to the motion of the target and tip.

The circular motion path is used to verify the found performance results, from different control algorithms, using the more simple straight path (Figure 6.7). The inverse kinematics control performs slightly better compared to PI with and without hysteresis compensation. The hysteresis compensation does not have a clear performance boost, as it had with the straight path. It should be noted, the inverse kinematic controller has some vibration around 3 seconds and is in general less smooth. This increases the chance of motion blur in the captured image.

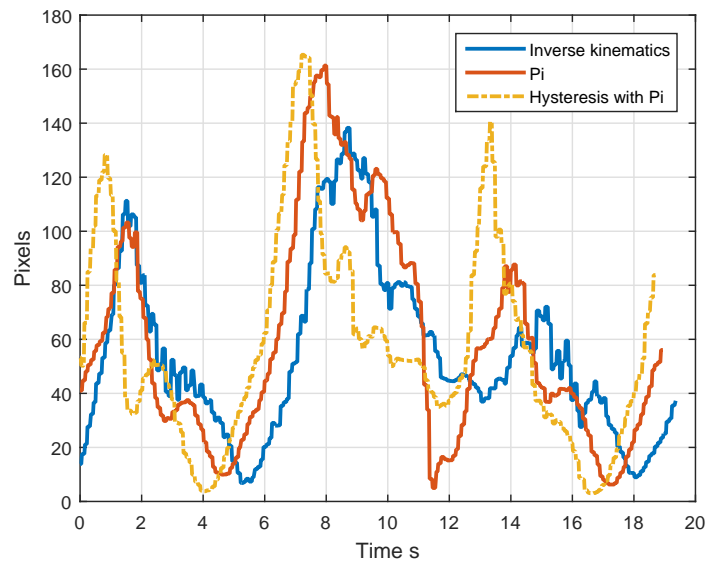


**Figure 6.7:** The plots show tracking error for 1 circular motion for different control algorithms.

Hysteresis compensation in the circular motion is analysed looking at both degrees of freedom separately. This shows the hysteresis compensation is working for both degrees of freedom. At 13 second, an extra peak shows up in the X direction of the hysteresis compensated control algorithm, this is the response to early switching the hysteresis compensation off.

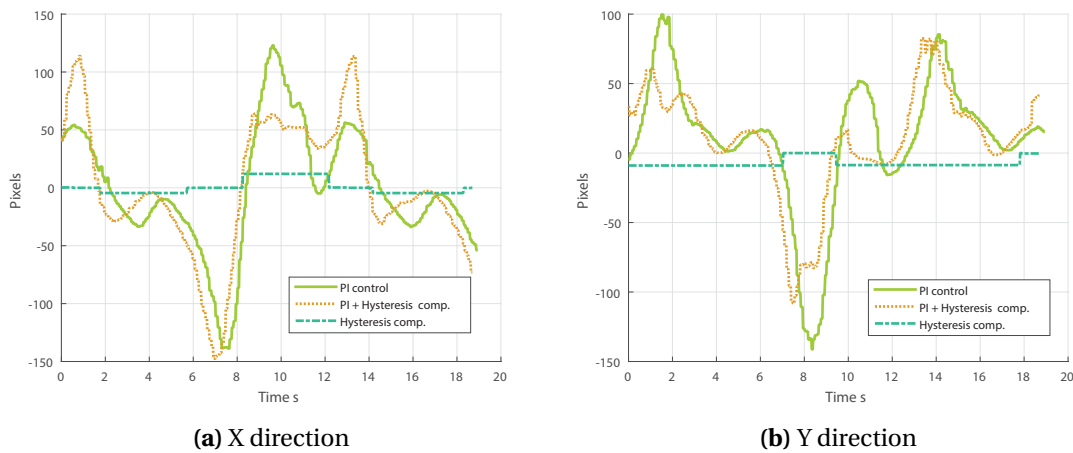


**Figure 6.8:** The tracking error plotted for 1 circular motion split in the x and y direction. The PI controller is compared to the PI controller with hysteresis compensation. The used hysteresis compensation during the control is also added to plot.

## 7 Conclusion

The aim of the project was to integrate target lock for endoscopes on the TeleFLEX set-up. The vision algorithm is integrated as native python extension. During the experiment, this proof to be a reliable connection, and easy to use. Different steering algorithms are designed and integrated in the current TeleFLEX setup. The experiment showed it was possible to automatically steer the tip of an endoscope, based on the input of the vision algorithm using the different designed auto steering algorithms.

The vision was mainly focused on a short computable time and high frame rate. The latency measurement showed short computable time does not grantee low latency in the control loop. Attempts to lower the latency were unsuccessful. The video encoder on the TeleFLEX is likely to be the limiting factor and adds most of the latency. The measured latency of 0.4 seconds is limiting the performance of the target lock.

The performance of different auto steering algorithms are tested and compared, using the experimental set-up. The straight path of the target also allowed the model to be validated, comparing the simulation results with the experiments.

The experiments showed that the hysteresis of an endoscope results in a large error of the tracked target, when direction was switched. The designed hysteresis compensation, showed improvement of the target lock using the straight path of the target. The more complex circular motion of the target showed hysteresis compensation can have unexpected behaviour. This should be studied further by performing experiments on the TeleFLEX model and real setup. The inverse kinematic controller showed comparable performance using the PI controller with hysteresis compensation, using purely feedback. The inverse kinematic control can be less fluent as can be seen in the circular motion of the target. This is likely to be caused by synchronisation issues between the motor position and camera image plane.

During the project, the OptiTrack is integrated into the TeleFLEX set-up to measure hysteresis of an endoscope. This allowed new hysteresis measurements, showing the hysteresis width is depending on both bedding degrees of the tip. New hysteresis measurement are used to make a model of an endoscope and TeleFLEX set-up. This allowed the different control strategies to be tested in simulation before integrating them in the real TeleFLEX set-up. The simulated target lock results, are compared to the real experiments. These results show the model has similar response compared to the real experiment. The model can be used to design control algorithms, and predict performance improvements.

## 8 Discussion and recommendations

The current experimental results show, the tip can track a target using auto steering and the vision algorithm. The current experiments are performed using a large target to maximize the reliability of the vision algorithm. This increased the distance between the tip and target. The distance should be reduced to approximately 1–2 cm to get more reliable result on performance of the target lock under more realistic circumstances. The closer target will result in smaller displacements of the target and tip. Hysteresis is expected to have relatively more effect under these small displacements. The hysteresis width is constant while the steering value decreases, and can become even smaller compared to the hysteresis width. As the distance between the camera and target shortens the sensitivity of the feedback will change, this result in a lower  $I$  action of the PI controller. A lower  $I$  action means hysteresis suppression using purley feedback takes longer. The inverse kinematic controller takes distance into account, possibly leading to better performance at close distance to the target.

The closer distance can be tested in simulation, it is recommended to verify the results on the real TeleFLEX set-up as well. To reduce the distance, a smaller target has to be printed. Initial test showed the small target was not robust, due to limitation of printing resolution. This is solved as the current vision implementation on the TeleFLEX set-up has a functional marker detection library [6]. These markers can be scaled to smaller sizes. The library has comparable performance in frame rate, as the currently used vision algorithm. Lighting of the target is still an issue and the target back light should be used. This marker detection library could also be used to validate the tracking algorithm as is done in [17], by placing the markers outside the tracking area. This a less complicated test set-up, using only the endoscope camera tracking, instead of mixing this with the OptiTrack tip orientation data.

The test environment should be increased in reality. This can be done limiting the distance between the target and the camera. Besides that, research is also required to parametrize the disturbance the target lock has to cancel. For example the target moves 2cm within 1 second, or the endoscope shaft rotating 10 degrees.

Currently the hysteresis compensation assumes the tip orientation can be predicated based on the input of the control handle. Outside disturbance could move the tip within the hysteresis plus deadband width without moving the control handle. This can results in rapid motion of the tip if the hysteresis is compensated using feed forward. The likelihood of this occurrence should be tested. This problem can only be solved by using an external sensor measuring the actual tip position. The current results of hysteresis suppression, show what kind of gain to expect when using hysteresis compensation.

The change of hysteresis due to bending of the endoscope shaft, is currently not modelled. However, there are some options to model this. The increase of hysteresis due to bending can probably be split in two regions. During the first region, increase of hysteresis is an effect of the increase in friction in the conduit cable while the deadband goes to zero, this can be parametrized in  $\mu_n$  in Equation (3.29). In the second region, the deadband is gone and the conduit cable pair starts to get pretension. This result in extra friction in the tip and conduit cable. This can be parametrized in  $\mu_n$  and  $F_n$  in Equation (3.29). This should also be used to further improve hysteresis compensation.

The experiments showed the current vision algorithm should be more robust. This algorithm is based on feature detection and matching the found features of the current frame  $X_n$  with the previous frame  $X_{n-1}$ . The features matched are filtered to get the correct displacement value. The target lock can be redesigned to be more robust by matching the found features in the capture image frame, to more frames in the history. This can be used for example, to

detect false positives as the matched feature translation detection of frame  $X_n$  to  $X_{n-1}$  should be equal to  $X_n$  to  $X_{n-2} + X_{n-1}$ . Performance should not be an issue as feature matching can be done in parallel on the Graphical Processing Unit.

## Bibliography

- [1] V. Agrawal, W. J. Peine, and B. Yao. Modeling of a closed loop cable-conduit transmission system. In *Robotics and Automation, 2008. ICRA 2008. IEEE International Conference on*, pages 3407–3412. IEEE, 2008.
- [2] S. Astanin. Optirx. <https://bitbucket.org/astanin/python-optirx/>, 2015. [Online; accessed 1-Juni-2015].
- [3] B. Bardou, F. Nageotte, P. Zanne, and M. De Mathelin. Design of a telemanipulated system for transluminal surgery. In *Engineering in Medicine and Biology Society, 2009. EMBC 2009. Annual International Conference of the IEEE*, pages 5577–5582. IEEE, 2009.
- [4] B. Bardou, F. Nageotte, P. Zanne, and M. De Mathelin. Improvements in the control of a flexible endoscopic system. In *Robotics and Automation (ICRA), 2012 IEEE International Conference on*, pages 3725–3732. IEEE, 2012.
- [5] D. B. Camarillo, C. F. Milne, C. R. Carlson, M. R. Zinn, and J. K. Salisbury. Mechanics modeling of tendon-driven continuum manipulators. *Robotics, IEEE Transactions on*, 24(6):1262–1273, 2008.
- [6] S. Garrido-Jurado, R. Muñoz-Salinas, F. J. Madrid-Cuevas, and M. J. Marín-Jiménez. Automatic generation and detection of highly reliable fiducial markers under occlusion. *Pattern Recognition*, 47(6):2280–2292, 2014.
- [7] M. W. Hannan and I. D. Walker. Kinematics and the implementation of an elephant’s trunk manipulator and other continuum style robots. *Journal of Robotic Systems*, 20(2):45–63, 2003.
- [8] M. Kaneko, M. Wada, H. Maekawa, and K. Tanie. A new consideration on tendon-tension control system of robot hands. In *Robotics and Automation, 1991. Proceedings., 1991 IEEE International Conference on*, pages 1028–1033. IEEE, 1991.
- [9] H. Kitagawa and Y. Ito. Bending section structure of endoscope, 2009. US Patent App. 20090209819.
- [10] L. Ott, F. Nageotte, P. Zanne, and M. De Mathelin. Robotic assistance to flexible endoscopy by physiological-motion tracking. *Robotics, IEEE Transactions on*, 27(2):346–359, 2011.
- [11] G. Palli and C. Melchiorri. Model and control of tendon-sheath transmission systems. In *Robotics and Automation, 2006. ICRA 2006. Proceedings 2006 IEEE International Conference on*, pages 988–993. IEEE, 2006.
- [12] R. Reilink. *Image-based robotic steering of advanced flexible endoscopes and instruments*. University of Twente, 2013.
- [13] E. Rozeboom, R. Reilink, Matthijs, P. Schwartz, P. Fockens, and I. Broeders. Unpublished, evaluation of tip bending response in clinically used endoscopes. 2015.
- [14] J. G. Ruiters. *Robotic flexible endoscope*. University of Twente, 2013.
- [15] N. Van der Stap, R. Reilink, S. Misra, I. Broeders, and F. Van der Heijden. The use of the focus of expansion for automated steering of flexible endoscopes. In *Biomedical Robotics and Biomechatronics (BioRob), 2012 4th IEEE RAS & EMBS International Conference on*, pages 13–18. IEEE, 2012.
- [16] D. J. S. Vera. Mejorando la tolerancia de la endoscopia digestiva. colonoscopios de rigidez variable. 2012.
- [17] L. M. Voskuilen. Target tracking for endoluminal interventions, 2015.